University of Alberta

Asymmetric Driver Behaviour-Based Algorithms for Estimating Real-Time Freeway Operational Capacity

by

Ying Luo

A thesis submitted to the Faculty of Graduate Studies and Research
in partial fulfillment of the requirements for the degree of

Master of Science

in

Transportation Engineering

Civil and Environmental Engineering

Fall 2013

Edmonton, Alberta

ABSTRACT

To mitigate recurrent and non-recurrent congestion, and to make full use of limited roadway capacity, numerous Active Traffic Demand Management (ATDM) strategies have been proposed, developed and implemented. Segment capacity, a basic input of ATDM predictive models, has been commonly considered a fixed value; however, this consideration does not allow for the probability that complex segment capacity may vary as prevailing traffic conditions vary. Limited research was found that develops analytical models for real-time capacity estimation. This thesis proposes an asymmetric driver behaviour-based algorithm to model multi-lane traffic flow dynamics. By considering car-following and lane-changing behaviours at critical freeway segments, i.e. active bottlenecks and Variable Speed Limit (VSL)-controlled segments, the proposed method obtains real-time freeway operational capacity estimation. The model parameters have been calibrated with field observations taken in Edmonton, Alberta, Canada. The results show that the proposed algorithm accurately estimates real-time operational capacity at complex freeway segments.

ACKNOWLEDGEMENT

It would not have been possible to finish my master thesis without the help and support of many people. First, I would like to thank my committee members for their guidance. I would like to express my grateful appreciation and respect to my supervisor, Dr. Zhijun (Tony) Qiu, who has given me valuable guidance, extensive support and great patience. It has been a memorable, delightful experience for me to work in Dr. Qiu's research group. The excellent research and collaboration environment gave me the opportunity to improve myself every day.

Special thanks go to my research teammates who will also be my lifelong friends. I would like to thank Dr. Jie Fang, Md Hadiuzzaman, and Xu Wang, who are knowledgeable in freeway research and have provided their valuable support to my research. I also would like to thank Dr. Pengfei Li, Xu Han, Gang Liu, Jing Cao, Elena Yin, Lin Shao, Michael Ge, Dr. Mingjun Liao, and Md Ahsanul Karim, who have always been generous offering their help in my field data collection and graduate studies. Sincere appreciation goes to Rochelle Borchman and Jeffrey King for providing patient help in writing academic papers.

Last but not least, I wish to express my deepest love to my parents, my younger sister, other family members and my friends in my home country; their love and care have been my constant support all of these years.

TABLE OF CONTENTS

LIST OF TABLES

LIST OF FIGURES

LIST OF ABBREVIATIONS

ATDM	Active Traffic Demand Management
VSL	Variable Speed Limit
MPC	Model Predictive Control
FD	Fundamental Diagram
HCM 2010	*The Highway Capacity Manual 2010*
NGSIM	Next Generation Simulation
WMD	Whitemud Drive
WB	westbound
EB	eastbound
AADT	Annual Average Daily Traffic
TMC	Traffic Management Center
OD	Origin-Destination
RMSE	Root-mean-square-error

CHAPTER 1. INTRODUCTION

This chapter presents the necessity of real-time capacity estimation for Active Traffic Demand Management (ATDM), and describes the motivations for this research. This chapter also introduces the present state and problems of capacity estimation methods in discretized traffic models.

1.1 Background

Active bottlenecks limit the traffic throughput and form an upstream queue. The maximum queue discharge flow is often lower than the segment capacity. This phenomenon is referred to as "capacity drop". According to their cause, active bottlenecks can be classified as recurrent or non-recurrent. Recurrent bottlenecks are activated by periodical, excessive traffic demand during peak hours. Non-recurrent bottlenecks are generally caused by an unpredictable incident that blocks traveling lanes and reduces freeway capacity.

To mitigate recurrent and non-recurrent congestion and to make full use of limited roadway capacity, numerous Active Traffic Demand Management (ATDM) strategies have been proposed, developed and implemented in freeway operations over the past few decades. Among these strategies, Variable Speed Limit (VSL) is one of the most effective controls for improving congested traffic conditions. The basic principle of VSL control is to mitigate traffic breakdown by lowering the posted speed limit: once the traffic demand exceeds the bottleneck capacity, a lower speed limit is posted approximately 500 metres (m) upstream of the bottleneck. By posting a lower speed limit, the time for arriving vehicles to

join the queue is delayed, which means that vehicles do not need to make sudden braking actions and, therefore, pass through the bottleneck more smoothly.

Hadiuzzaman et al. [1] proposed a model predictive control (MPC)-based VSL control to improve freeway mobility. This strategy was intended to be implemented on Whitemud Drive (WMD) in Edmonton, Alberta, Canada. The proposed MPC-based VSL control contained four major components: 1) a predictive model extended from METANET [2]; 2) an objective function; 3) an optimal speed limit searching tool; and 4) the control action. The predictive model estimated the upcoming (within the next few minutes) traffic condition. The controller updated the optimal speed limit according to the optimization of the corridor flow efficiency, according to the prediction. Hence, the predictive model had a notable impact on this feedback control. The METANET model is the discretized formulation of Payne's second order traffic model [2, 3]. The discretized formulation was derived from the continuum model by partial differential equations. The model performances are sensitive to the boundary conditions. Segment capacity, as one of the boundary conditions of the predictive model, influences model accuracy, as well as the control performance.

Previously, the capacity in the METANET model was calibrated from a fundamental diagram (FD: flow vs. density). For the impact of different speed limits, the study assumed that the capacity varies under different speed limits. For active bottlenecks, the dropped capacity was modeled by a fraction term θ, as shown in Figure 1 [1].

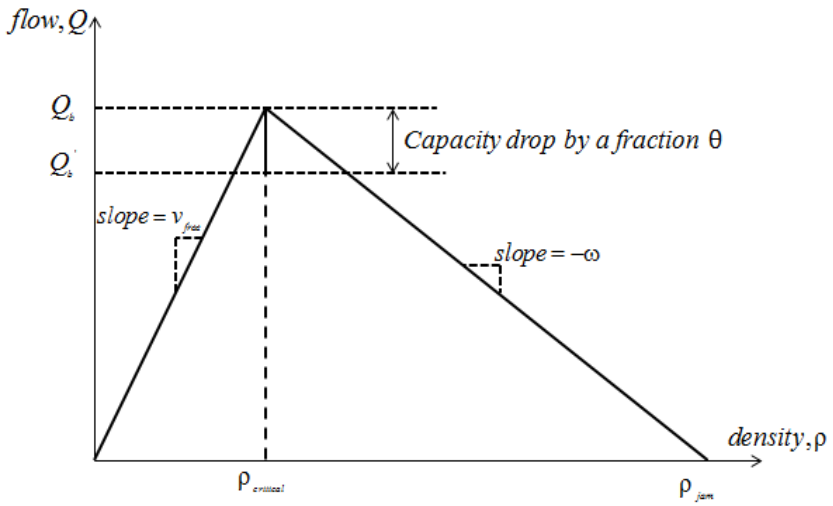

Figure 1 FD assumption for bottleneck locations [1]

1.2 Problem Statement and Research Motivation

Before stating the problem and research motivation, the definition of capacity should be clarified. As emphasized by Minderhoud et al. [4], capacity should be distinguished as design capacity, strategic capacity and operational capacity. Among these, the operational capacity dynamically changes according to prevailing conditions and possesses research value for real-time freeway controls. Hence, the "capacity" discussed in this thesis is defined as real-time maximum discharge flow on urban freeways, which is "operational capacity" (sometimes also called "effective capacity" [5]).

1.2.1 Problem of Using Static Capacity Value at Complex Freeway Segments

In existing MPC-based VSL controls [1, 6, 7] , researchers employed static FDs (flow vs. density curve) for each segment under each different speed limit. Transition flow at each time step was represented as the minimum of three terms: 1) the flow at the current link; 2) the capacity of the downstream link; and 3) the supply from the downstream. These three terms were each estimated from the FD,

and the segment capacity in each scenario was assumed as the tip point of the FD. However, this assumption has certain limitations:

- The FDs represent the equilibrium traffic condition. For freeway bottlenecks with complex geometric characteristics and/or driving behaviours, the traffic stream is non-steady in nature. Since the prediction time step was often short in MPC-based VSL, the operational capacity cannot always be considered constant;
- Freeway bottlenecks can be activated by excessive traffic demand or by unpredictable incidents. At bottlenecks, the maximum queue discharge flow is often lower than the segment capacity [8, 9] .This phenomenon is referred to as "capacity drop". For different types of bottlenecks (merging, diverging, lane-drop and non-recurrent), the magnitude of the capacity drop was not theoretically represented in the existing traffic models;
- For VSL-controlled segments, existing predictive models [1, 6, 7] employed static flow-density curves for each speed limit. However, when the speed limit is updated over a short time period, the operational capacity fluctuates because of drivers' response to the posted speed limit. Modeling the drivers' dynamic behaviour to VSL is necessary to understand the aggregated flow behaviour under VSL control.

1.2.2 Problem of Existing Capacity Estimation Techniques

The Highway Capacity Manual (HCM) 2010 stated two factors that influence freeway operation: "The traffic stream on uninterrupted-flow facilities is the result of individual vehicles' interaction with each other and the facility's geometric

characteristics." (vol.1, pp8-3) Therefore, a good traffic flow model needs to consider drivers' interactions and geometric characteristics. The capacity estimation methods in the *HCM 2010* consider segment geometry characteristics and traffic compositions. The impact of individual vehicle interactions, especially at complex freeway segments, was not addressed. Another stream of capacity estimation was mostly based on a statistical analysis regarding the relationship between capacity drop and pre-breakdown flow, speed and density [10]. This study produced only location-specific models and did not produce analytical models for different prevailing conditions.

1.2.3 Research Motivation

To refine the aforementioned disadvantages of using a static capacity value, this research proposes a new method for estimating real-time freeway operational capacity. The proposed method is capable of addressing the impact of drivers' interactions and their reaction to a segment's geometric characteristics at critical freeway segments, i.e., different types of active bottlenecks and VSL-controlled segments.

This research focuses on modeling drivers' behaviours at freeway merging, diverging, lane-drop and non-recurrent bottlenecks, as well as VSL-controlled locations. The operational capacity is considered the result of car-following and lane-changing behaviours at the studied segments. The obtained dynamic capacity value can be used in the boundary condition of the METANET model, employed by a previously proposed VSL control [1].

Drivers' acceleration and deceleration behaviors are considered asymmetric—a consideration established in 1965 and widely accepted; however, limited research was found to model the asymmetric phenomenon. The principle of asymmetric behaviour is that drivers are used to having a larger headway when accelerating compared to when decelerating, given the same speed. This assumption results in hysteresis in the FDs [11, 12, 13, 14].

1.3 Research Objectives and Scope

1.3.1 Research Objectives

This study develops a new method for estimating operational capacity at critical freeway segments considering both drivers' interactions and segment geometries. The research has three specific objectives:

- Develop analytical microscopic models that consider drivers' interactions, as well as their reaction to VSL command and bottleneck geometric features;
- Develop online traffic state estimation algorithms based on microscopic models with real-time traffic data collected by inductive loop detectors; and
- Obtain real-time operational capacity values at critical freeway segments.

1.3.2 Research Scope

To improve the performance of the previously proposed VSL control [1], this study aims to estimate real-time operational capacity at several complex segments on the study corridor. Flow dynamics at four types of freeway segments are

investigated: merge, diverge, non-recurrent bottlenecks (lane-drop), and VSL-controlled segments. With the available data sources, this research has several considerations:

- This research models traffic instability caused by vehicles' frequent lane-changing, acceleration and deceleration, which is necessary for capacity estimation at the studied freeway segments;
- This research employs only one set of microscopic model parameters to represent average driver characteristics at the studied freeway segment;
- For merging bottlenecks, the operational capacity is estimated as a result of merging impact and merging ratio;
- For diverging bottlenecks, the operational capacity is estimated as a result of diverging impact and diverging ratio;
- For lane-drop bottlenecks, the operational capacity is estimated as a result of drivers' reaction to lane-drop. The impact of a non-recurrent bottleneck is assumed as lane block at incident locations, which can be considered the same as lane-drop bottlenecks;
- For VSL-controlled segments, the operational capacity is estimated by drivers' response to speed limits and their car-following behaviors.

1.4 Structure of Thesis

This research is presented in five sections:

Chapter one introduces the background and motivation of this research; the research objectives are also clearly defined, as is the study scope.

Chapter two presents a literature review of the capacity estimation methods. The existing research is classified into three categories: 1) empirical observation-based methods; 2) macroscopic analytical model-based methods; and 3) behaviour-based microscopic models. The advantages and disadvantages of these studies are discussed. The reasoning behind using asymmetric driving behaviours is stated at the end of this chapter.

Chapter three is the key part of this thesis. The car-following and lane-changing model under asymmetric driving behaviour theory is presented first. According to the car-following and lane-changing rules, the capacity estimation algorithms at the studied freeway segments are developed. The model calibration and validation method is then presented.

Chapter four summarizes the results of the field data collection and model calibration, as well as introduces the study corridor (Whitemud Drive in the City of Edmonton, Alberta, Canada), the data collection process and the parameter estimation results.

Chapter five presents the queue discharge flow estimation for the studied segments. From the queue discharge flow, capacity value at the complex freeway segments is obtained. The proposed bottleneck capacity estimation algorithm shows its flexibility in capacity estimation at both recurrent and non-recurrent bottlenecks compared to empirical methods. The proposed VSL operational capacity estimation algorithm produces results consistent with field observations conducted on European highways.

Chapter six summarizes the major findings and contributions of this research. This chapter also presents the limitations of this study, which leads to future work and recommendations for related topics.

CHAPTER 2. LITERATURE REVIEW

This chapter summarizes the existing freeway capacity estimation techniques, which are classified into three categories: 1) empirical observation-based methods; 2) macroscopic analytical model-based methods; and 3) behaviour-based microscopic models. The advantages and disadvantages of these studies are discussed. The reasoning behind using asymmetric driving behaviours is stated at the end of this chapter.

2.1 Freeway Capacity Definitions and Characteristics

Before discussing the existing freeway capacity estimation methods, this section gives a brief introduction about the capacity definitions presented in the *HCM 2010*. This section then summarizes the contributive factors of freeway operational capacity.

2.1.1 Capacity on Freeway Critical Segments

This research focuses on capacity estimation on several critical freeway segments. The *HCM 2010* clearly presents the necessity of analyzing the capacity on critical segments, which determine the entire corridor's capacity:

> Freeway facility capacity is the capacity of the critical segment among those segments composing the defined facility. This capacity must, for analysis purposes, be compared with the demand flow rate on the critical segment. The critical segment is defined as the segment that will break down first, given that all traffic, roadway, and control conditions do not change, including the spatial distribution of demands on each component segment. (vol.2, pp10-6)

2.1.2 "Two Capacity Phenomenon"—Capacity Drop at Freeway Bottlenecks

The HCM 2010 clarifies the definition of queue discharge flow:

> A traffic flow that has passed through a bottleneck and, in absence of another bottleneck downstream, is accelerating back to the free-flow speed of the freeway. Queue discharge flow is characterized by relatively stable flow as long as the effects of another bottleneck downstream are not present. (vol.1, pp.2-12)

Several empirical studies have found that the bottleneck queue discharge flow rate decreases after the onset of a queue. Researchers reported 5-17% capacity drop at freeway merge bottlenecks [9, 15, 16] and approximately 10% at freeway lane-drop bottlenecks [8, 9]. The main reason of capacity drop was demonstrated in later studies: Laval and Daganzo found that the contributing factors of bottleneck capacity drop are frequent lane-changing and vehicle acceleration capability [17, 18]

Both of the aforementioned field studies and the *HCM 2010* emphasized the necessity of investigating freeway bottleneck traffic instability caused by frequent lane-changing, acceleration and deceleration, which is the main objective of this research.

2.1.3 The Impact of ATDM on Freeway Capacity

The effect of ATDM on highway capacity was presented in the *HCM 2010*: "ATDM measures can influence both the nature of demand for the facility and the ability of the facility to deliver the capacity tailored to serve the demand. ATM measures can improve facility performance, sometimes significantly" (vol.2, pp.10-14).

The *HCM 2010* pointed out that VSL was reducing mainly the crash probability caused by sudden braking; hence, traffic breakdowns were delayed. To the best of the authors' knowledge, only one study investigated the capacity effects of VSL from field observations. Papageorgiou et al. [19] conducted a comprehensive study on the flow impact of VSL. They found that by reducing speed limits, the average speed at under-critical occupancy decreased, while the critical density increased. However, the throughput of the VSL-controlled segment may slightly decrease during transitions—after that, segment capacity may increase in some scenarios; hence, the traffic flow impact of VSL requires a measurement methodology.

2.2 Empirical Models for Capacity Estimation

There are two empirical approaches to determine freeway capacities: 1) indirect methods, such as the *HCM 2010* procedure; and 2) the stochastic regression approach. Many capacity analysis studies performed a statistical analysis of the observed traffic variables, i.e. headway, flow, speed, density. Researchers were focused mainly on the randomness of capacity with respect to pre-breakdown traffic states.

2.2.1 Capacity Estimation Method in the HCM

The *HCM 2010* provided a detailed procedure to compute capacities at general freeway diverging, merging and weaving sections in prevailing conditions. The *HCM 2010* method considers geometric features, weather conditions, lighting conditions and work-zone activities. The determining factor of freeway capacity is free-flow speed, which is a function of a freeway's geometric features, such as

lane width, shoulder width and ramp density. The *HCM 2010* methodologies have some limitations; for example, the capacity drop caused by vehicles' interactions at complex freeway segments was not considered.

2.2.2 Capacity Estimation with Headway Observation

The basic equation of this method is $q = 3600 / \bar{h}$, where, q is flow in vehicles per hour and $\bar{h}$ is the mean time headway in seconds per vehicle. The stochastic distributions of mean headway at near capacity regimes were estimated. The density function of the headway distribution is determined by the headway of two vehicle groups: bounded vehicles and free driving vehicles [20]. The general equation of this method is expressed as [20]:

$$f(t) = \psi \times g(t) + (1 - \psi) \times h(t) \tag{2-1}$$

where,

$f(t)$ = the probability density function (PDF) of critical headway;

$g(t)$ = the PDF of car-following vehicles;

$h(t)$ = the PDF of free driving vehicles; and

ψ = the proportion of car-following vehicles.

The advantage of this method is that observation bias is avoided. The censored data at the under-capacity condition will not lead to underestimation. The limitation of this method is that the distribution of $g(t)$ is assumed to be similar in both the intensive traffic condition and in the near-capacity traffic condition. Hence, the roadway capacity is always overestimated [4].

2.2.3 Capacity Estimation with Flow Observation

Several studies investigated capacity distribution. It was believed that traffic breakdown and recovery follows the transition from an uncongested state to a congested state, and then a converse process from congestion to non-congestion. The capacity was defined as the maximum flow rate before congestion occurs. The capacity distribution function was expressed as [10]:

$$F_c(q) = p(c \le q) \tag{2-2}$$

where,

p = the probability of traffic breakdown caused by exceeded demand;

c = the capacity value in vehicles per hour; and

q = the observed flow rate in vehicles per hour.

The basic assumption of this method is that the momentary capacity of the studied freeway section is the maximum traffic volume observed before a breakdown occurs. The probability function $p(\bullet)$ was formulated in several ways. Persaud et al. [16] categorized flow by group, and for each flow rate group, the number of breakdowns was counted. The breakdown probability at this flow rate was calculated as the breakdown number over the total number of observations. However, this method underestimated capacity values, because the highest flow rate was observed only during the data collection period, which leads to observational bias. To overcome this limitation, a nonparametric method, which was called the product-limit method of Kaplan and Meier, was proposed to estimate the capacity distribution function [10]. This method considered uncensored flow data, and produced reasonable estimation results.

Random distribution fittings were performed after obtaining the capacity density distribution. Brilon et al. [21] found that freeway capacity was a Weibull-distributed random variable. Kim et al. [22] used the Weibull, Gaussian and logistic distribution to fit the capacity probability function. It was found that the Gaussian distribution was the best-fit model.

2.2.4 Capacity Estimation with Density and Speed Observation

Chow et. al. [24] adopted a bivariate Weibull distribution with mean speed and occupancy of incoming traffic to find the probability of traffic breakdown. Ishak et. al. [25] used 30-second speed data as an indicator of incoming traffic states, and estimated negative and positive transition probability of traffic speed and the speed transition curve to capture the nature of traffic breakdown and recovery.

2.3 Analytical Models for Capacity Estimation

2.3.1 Macroscopic Analytical Models for Capacity Estimation

- ***Fundamental Diagram-based Capacity Estimation***

FD calibration is a widely used approach to estimate location-specific capacity. This method requires sufficient observation of traffic data to determine critical density. Capacity is obtained by observing the maximum flow at free flow speed in a critical density situation.

The FD can model both bottleneck capacity and VSL-controlled segments. All existing macroscopic traffic models determine capacities with FD calibration. For bottleneck capacity, fraction terms could be added to represent capacity drops [1]. For VSL control, Hegyi et al. [6] and Carlson et al. [7] rescaled the flow-

density diagram (fundamental diagram). Hegyi et al. [6] assumed that the free flow speed always equals the posted speed limit; at a lower speed limit, the critical density slightly increased. Further, according to field observations on the European Motorway [19] , Carlson et al. [7] rescaled the FD in VSL control. The modifications included all the observed VSL impacts from European field studies [19]: decreased mean speed at uncongested regimes and increased critical density. The difference between the Hegyi et al. and the Carlson et al. model is that the Carlson et al. model's FDs have cross points at the critical density region in different speed limits, which means, in some cases, lowering the speed limit will not decrease operational capacity. These two studies can be considered benchmarks for modeling VSL impact on traffic flow. Heygi et al. and Carlson et al. addressed the equilibrium traffic state estimation under VSL control, with the assumption that the traffic states did not substantially change. Another study from Wang et al. [26] also derived a second-order model to account for transition effects. They assumed that drivers' reaction time to the speed limit change was longer than that of the leading car. Therefore, a term was added to describe the drivers' behaviour when the VSL command is lower than their current driving speed. The modification gave accurate simulation results.

If sufficient field observation data is available, FD calibration is a reasonable option; however, it has limitations: the estimated capacity is highly dependent on the speed-density relation assumption; each pair of the speed-density observations may occur differently in different situations because of the dynamic nature of the prevailing conditions, which makes the critical density

difficult to measure. Furthermore, insufficient observation data at the critical density region causes estimation bias.

- ***Optimization Method***

At complex freeway segments, the through flow and diverging flow conflict with each other, which has a notable impact on the freeway capacity. To study the impact of larger gaps for conflicting vehicles, Lertworawanich et al. [27, 28] proposed to consider the maximum flow that a segment can accommodate as a linear optimization problem. The constraints are the minimum gap for those conflicting vehicles. As Figure 2 illustrates, the general equations of this optimization problem are [27]:

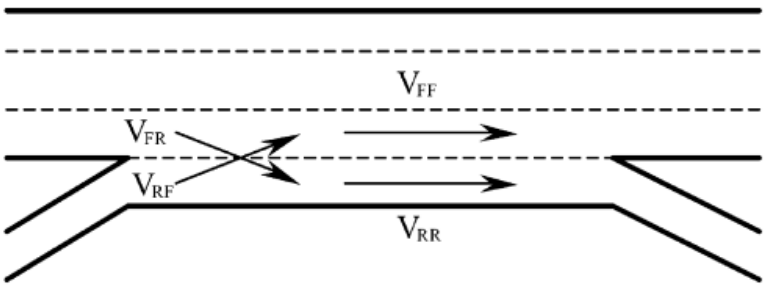

Figure 2 Sketch of a ramp weave [27]

$$\text{Capacity} = \max(V_{FF}+V_{RF}+V_{RR}+V_{FR}) \quad (2\text{-}3)$$

Subject to:

- The basic freeway capacity (BFC) constraint: $V_{FF}+ V_{RF} \le$ BFC; $V_{RR}+V_{FR} \le$ BFC; $V_{FF}+ V_{FR} \le$ BFC; $V_{RF}+V_{RR} \le$ BFC;
- Demand proportion constraint: $V_{RF}/ (V_{RF}+V_{RR}) = W_0$; $V_{FR}/ (V_{FF}+ V_{FR}) = W_1$;
- Potential capacity constraint: $V_{FF} \le$ BFC; $V_{RR} \le$ BFC; $V_{RF} \le \max(V_{RF})$; $V_{FR} \le \max(V_{FR})$;

where,

V_{FF} = the through flow;

V_{RR} = the flow from on-ramp to off-ramp;

V_{RF} = the merging flow; and

V_{FR} = the diverging flow.

Capacity of merging and diverging of the freeway max(V_{RF}), max(V_{FR}) were estimated via the gap acceptance theory.

The major challenge of this model is how to determine the merging and diverging capacity, which are both highly dependent on the merging and diverging demand, the number of freeway lanes and the vehicles' gap acceptance behaviors.

2.3.2 Microscopic Analytical Models for Capacity Estimation

Usually, microscopic analytical methods are all simulation studies, which require that the proposed microscopic model well-represents the real-world traffic with reasonable assumptions. Compared to the *HCM 2010* methods, microscopic simulations are able to accommodate the impact of driving behaviors. In simulation, freeway capacity is typically an assumption of drivers' car-following and lane-changing behavior.

Recently, much microscopic simulation software has been developed for comprehensive studies on traffic flow. Vehicles' longitudinal and latitudinal behaviours were coded based on assumptions. The simulation results are highly dependent on the car-following models and lane-changing models; hence, there is a necessity for the upcoming summary of some benchmark theories for modeling

vehicles' longitudinal and latitudinal behaviors. After that summary, the general process of determining roadway capacity from simulation results is presented.

- ***Modeling Vehicles' Longitudinal Behaviour and Corresponding Capacity***

Vehicles' longitudinal behaviour is key when determining roadway capacity. Vehicles' car-following spacing directly influences the critical density and maximum number of vehicles passing through a roadway segment. From car-following models, the base capacity can be determined.

Newell's simplified car-following rule [29] is the simplest model with the least number of parameters. This model describes a follower's position as a spatial-temporal transformation of leading vehicles. This lower-order model falls into the trajectory translation category and is consistent with the kinematic wave theory at a macroscopic level. Newell suggested that this model only apply to homogeneous highways. To validate Newell's car-following model, Ahn et. al. [30] used a bivariate normal distribution of lane-by-lane, τ_n and d_n. The model estimations were consistent with field data observed from two signalized intersections. Later, longitudinal inhomogeneity in the traffic stream was considered.

Kim and Zhang [31] used stochastic gap time as a basic variable in their model, which had the same wave propagation mechanism as Newell's. They showed that stochastic driver reaction times led to random growth and decays of traffic disturbances. Laval and Leclercq [32] stated that the vehicle trajectories from field observations agree well with Newell's car-following model before the

consideration of traffic oscillations and lane-changing behaviors. They extended Newell's model by introducing a new term to capture behaviour in non-equilibrium traffic states.

Some researchers found that congested traffic instability was caused by acceleration and deceleration, which implied drivers' acceleration and deceleration behaviours are asymmetric. Earlier observations found that drivers were used to having a larger headway when accelerating compared to when decelerating, given the same speed. This assumption results in hysteresis in the FDs [11, 12, 13, 14, 33]. Treiterer and Myers [34] named the loop in the flow-density diagram: "Traffic Hysteresis Phenomenon". Based on the asymmetry assumption, Zhang claimed that "acceleration, deceleration and equilibrium flow should be distinguished in obtaining speed-density relationships [35]." Recently, Yeo [14] proposed the asymmetric driving behaviour theory. In Yeo's study, there are two curves along the congestion side of the FD, namely A-curve (acceleration curve) and D-curve (deceleration curve). From a microscopic point of view, the speed-spacing relations of acceleration and deceleration are different. Yeo derived this relation and adjusted it as an extension of Newell's simplified car-following model [29]—an extension in which wave travel time τ_n and wave travel distance d_n in the acceleration and deceleration processes are different. Zhang and Kim [36] developed a car-following theory with multiphase vehicular traffic flow. Vehicles changed their car following behaviour between coasting, acceleration and deceleration phases. This theory produced capacity drop and hysteresis, but was not validated by field data. Later, Chen et al. [37] proposed a dynamic temporal-

spatial queuing model, which considers asymmetric driving behaviors; however, this model did not consider the lane-changing impact.

- ***Modeling Vehicles' Longitudinal and Lateral Behaviour and Corresponding Capacity***

Studies [32, 38] showed that Newell's simplified car-following theory fails in the context of frequent lane-changing manoeuvres. To replicate real-world traffic congestion, researchers modeled vehicles' latitudinal interactions.

The existing lane-changing models fall into two streams: 1) one stream explicitly describes interactions in free, cooperative and forced lane-changing situations; however, more parameters are required [39]; and 2) one stream categorizes lane-changing into mandatory and discretionary actions, which needs fewer parameters and is more suitable for flow estimation [17, 18]. For example, in 2006, Laval and Daganzo [17] proposed a lane-changing model to ensure consistency between micro and macro measurements. They converted lane-specific macroscopic variables to the lane-changing rate, and discretized the lane-changing rate into the lane-changing time-space point. This model can be applied on freeway sections far away from the off-ramps, where the main purpose of lane-changing is to increase speed. The results were consistent with observations taken from merge and lane-drop bottlenecks.

A driver's behaviour immediately after lane-changing is a contributing factor to influence operational capacity at complex freeway segments. Several studies have proposed mathematical models for describing a vehicle's car-following behaviours immediately after lane-changing. Based on the lane-

changing model proposed by Laval and Daganzo [17] and the moving bottleneck (vehicles that have limited acceleration capacity) model, Laval et al. [18] added another parameter to measure the relaxation impact. This relaxation model improves the bottleneck flow prediction. Laval interpreted the relaxation parameter as the speed difference between the leader and the follower after lane-changing. This speed difference was proposed to be approximately 2 kilometers per hour (km/h), and helps the follower achieve equilibrium spacing. Yeo [14] explained that if the incoming spacing of lane-changing vehicles is too small, then a vehicle must decelerate (relaxation phase), whereas if the spacing is large enough, relaxation is not needed. Hence, compared to Laval's model [18] , Yeo's theory has the flexibility to model the car-following and lane-changing rules in stop-and-go traffic. Yeo [40] also proposed a behavioural-based algorithm for oversaturated freeways. Yeo adopted a short gap model for lane-changing vehicles, which is quite similar to the asymmetric theory he proposed. This study was validated with Next Generation Simulation (NGSIM) trajectory data and loop detector data.

- ***Modeling Vehicles' Behaviour when Decreasing or Increasing Speed Limits***

Drivers' response to VSL is a critical factor in the real-world implementation of ATDM-VSL controls. Mean speed and corresponding critical density are dynamically changed because of variable speed limits. Hence, the roadway capacity changes when a different speed command is posted.

There is no behaviour-based microscopic model proposed for VSL-controlled segments. In existing VSL designs, only Hegyi [6] introduces a driver's compliance factor to constrain the mean speed at VSL-controlled segments, but the corresponding capacity was modeled by rescaling FDs. Kwon et al. [23] investigated drivers' compliance at a VSL-controlled work zone. They found that when the difference increased between the posted VSL and the upstream static speed limit, drivers' compliance to the VSL decreased. Rämä [41] investigated a road that employed weather-controlled VSL. He found that in clear weather conditions, fewer drivers decreased their speed on a VSL-controlled road compared to when on a road that carries an equivalent static speed limit. For this reason, we cannot simply adopt the compliance analysis for static speed limits to a VSL scenario.

- ***General Process of Determining Roadway Capacity from Microscopic Simulation***

From existing microscopic model-based studies, the actual freeway capacity is determined by six steps:

1. Determine car-following, lane-changing, gap acceptance models;
2. Collect field data and calibrate models for different locations;
3. Compute vehicle's position at each time step from proposed models;
4. Obtain vehicle trajectories and point-based accumulative vehicle counts;
5. Determine the capacity analysis points or section;
6. Determine the aggregation level, which is usually greater than 1 minute (min).

Among these steps, 5 and 6 are the most important for capacity analysis [4, 21]. The best observation point for capacity analysis is the segment's critical points, which are the first places that traffic breakdown occurs. In the *HCM 2010* methodologies, 15 minutes (min) is the time interval for capacity analysis. However, from field observation, the measured capacity value in 15 min is much lower than the actual capacity value. If the aggregation level is too small, for example, less than one min, then the measured capacity is highly dependent on the vehicle arrival type.

2.4 Summary of Literature Review and Research Implications

2.4.1 Summary of Literature Review

In the literature review, strengths and limitations of existing capacity estimation methods were discussed. Table 1 is a summary of those strengths and limitations of the state-of-the-art capacity estimation models with respect to their flexibility with the study objectives.

Table 1 Summary of literature review

	Methodology	Strengths	Limitations
Empirical Models	*HCM 2010* Methodologies	The most detailed guideline for adjusting capacity in prevailing conditions	Not flexible with modeling speed limit impact and active bottlenecks
	Headway observation-based	Data requirement is easy to meet; Observation bias is avoided;	Not flexible with modeling speed limit impact and active bottlenecks
	Flow, Density, and Speed observation-based	Easy to compute; Obtains capacity distributions	Sufficient field observations are needed to avoid bias.
Macroscopic Analytical Models	FD-based	Straightforward; Flexible with modeling speed limit impact and active bottlenecks	Observational bias exists; Only represents equilibrium state
	Optimization Method	Flexible with modeling real-time capacity at active bottlenecks	Merging and diverging capacity is difficult to determine in macroscopic representatives
Microscopic Analytical Models	Longitudinal Behaviour-based	Acceleration and deceleration impact on traffic flow is considered	High requirement of model parameters; Lane-changing impact at bottlenecks are not considered
	Longitudinal and Latitudinal behaviour-based	Lane-changing impact is considered	Highest requirement of model parameters

2.4.2 Research Implications

The major purpose of this study is to obtain a real-time freeway operational capacity estimation considering traffic instability caused by sudden geometry

change and VSL control. To fulfill the study purpose, four factors need to be considered in this research:

- Acceleration and deceleration caused by VSL, and lane-changing caused by roadway geometric changes are the main factors influencing critical segments. Considering the microscopic traffic models' flexibility in capturing the flow dynamics at complex freeway segments, integration of the car-following and the lane-changing model is needed in this study;
- Considering the limited data sources, microscopic models with fewer parameters, such as Newell's car-following model and Laval's lane-changing model, are preferred;
- Since Yeo's asymmetric driving behaviour theory has the flexibility to model vehicles' lane-changing, acceleration and deceleration, this research will adopt the asymmetric assumptions in the microscopic models. Previously, Yeo's theory was validated by NGSIM trajectory data, but no qualitative analysis was performed [14]. Hence, the first potential contribution of this thesis is to fill this gap by developing a car-following and lane-changing model under the asymmetric theory, and assessing the model performance with field data collected from WMD in the city of Edmonton;
- Since the major objective of ATDM is to make full use of limited roadway capacity, it is necessary to investigate the flow dynamics at the upstream of active bottlenecks. Chen's queue model [37] was the most flexible in obtaining real-time wave evolutions and dissipations; however, that study

only considered longitudinal behaviors. This paper will move that beyond by considering lane-changing impact.

To conclude, this paper will adopt Chen's wave propagation algorithm under Yeo's asymmetric driving behaviour theory. Car-following and lane-changing behaviours are considered. This approach will be flexible enough to model the flow impact of freeway bottlenecks and variable speed limit commands.

CHAPTER 3. METHODOLOGY

This chapter describes the car-following and lane-changing model under the asymmetric behaviour assumption. The physical properties of these models are interpreted in detail. Then, a wave propagation algorithm, extended from Chen's queue model [37] is presented. The application of the algorithm is to model the flow dynamics at different types of bottlenecks and VSL-controlled segments.

3.1 Asymmetric Car-Following Model

3.1.1 Base Model: Newell's Car-Following Model

Before introducing the asymmetric car-following rule, this section explains Newell's car-following model [29], which is the benchmark model consistent with the kinematic wave theory. The general equation for Newell's car-following model is written as follows [29]:

$$x_n(t+\Delta t) = min\{\underbrace{x_n(t)+u\Delta t}_{freeflow}, \underbrace{x_{n-1}(t+\Delta t-\tau_n)-d_n}_{Congestion}\} \qquad (3\text{-}1)$$

where,

x_n = position of the follower;

x_{n-1} = position of the leader;

τ_n = actual reaction time for n^{th} vehicle;

d_n = wave travel distance (jam spacing);

Δt = time step; and

u = free flow speed.

As Figure 3 (a) shows, Newell's car-following model assumes a linear relation between vehicle spacing and the following vehicle's velocity. If the leader changes its speed, the follower will change its speed after τ_n and the wave travel distance will be d_n (Figure 3 (b)). Here, τ_n is referred to as the follower's actual action time. One distinct advantage of Newell's model is that only two parameters [τ_n d_n] are required, which are both simple to obtain from field data. Also, this model well explains wave propagation. Newell made piece-wise linear approximations of vehicle trajectories, which do not explicitly reflect the vehicles' actual positions, but will not influence the macroscopic estimations; hence Newell's theory is ideal for an equilibrium state.

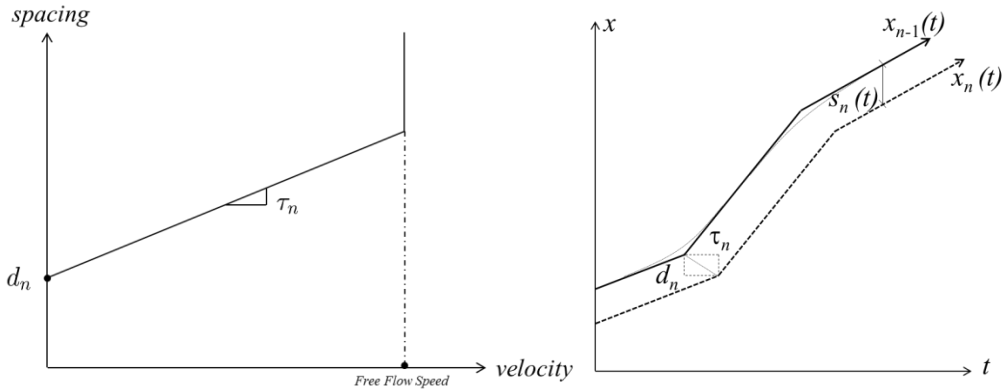

(a) (b)

(a) Relation between spacing and velocity in Newell's Car-Following Model;

(b) Piece-wise linear approximation to vehicle trajectories in Newell's model [14]

Figure 3 Spacing-speed relation and vehicle trajectory plot in Newell's model

3.1.2 Extending Newell's Car-Following Model in the Asymmetric Theory

Yeo proposed an asymmetric theory and extended the car-following rule based on two curve assumptions [14]. As Figure 4 (a) shows, Yeo assumes that the spacing-speed relations are different in the acceleration and the deceleration process. If the

leader changes speed, then the follower will change speed after coasting time plus action time, which is called "actual reaction time" in acceleration and deceleration. Here, the jam spacing is also different in acceleration and deceleration, which is easily observed at signal-controlled intersections.

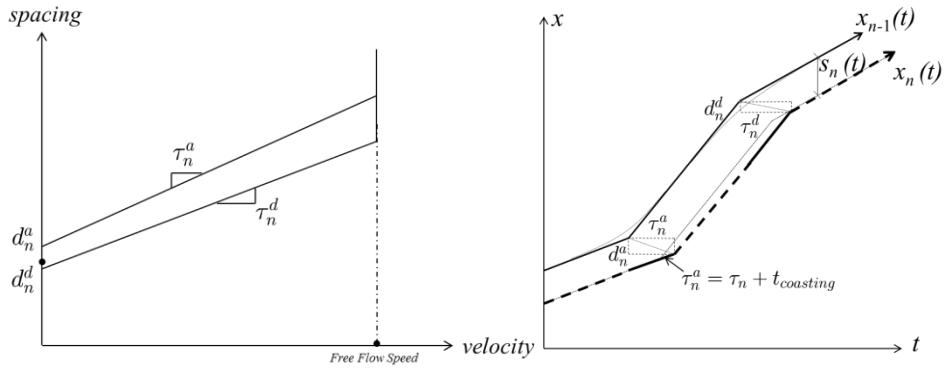

(a) (b)

(a) Relation between spacing and velocity in Asymmetric Theory (32);

(b) Piece-wise linear approximation to vehicle trajectories in Asymmetric Theory

Figure 4 Spacing-speed relation and vehicle trajectory plot in Asymmetric Theory

3.1.3 Interpretation of Model Properties

- ***Drivers' Aggressiveness***

As Figure 5 shows, the proposed asymmetric car-following theory can model drivers' aggressiveness. Aggressive drivers prefer to drive at a higher speed when free flowing, and they tend to follow too close to leading vehicles [14].

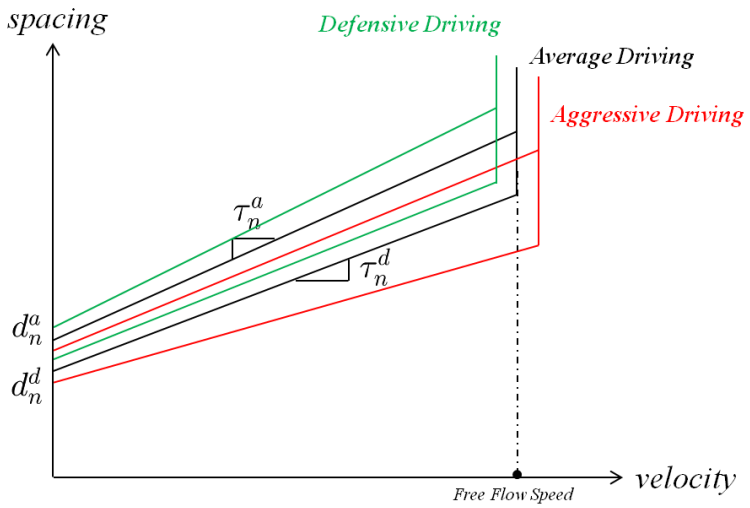

Figure 5 Spacing-velocity relation considering drivers' aggressiveness [14]

Drivers' aggressiveness can be modeled by changing five parameters: 1) free flow speed (u_n); 2) jam spacing when accelerating (d_n^a); 3) jam spacing when decelerating (d_n^a); 4) actual reaction time for acceleration (τ_n^a); and 5) actual reaction time for deceleration (τ_n^d).

- ***Impact of Heavy Vehicles***

The presence of heavy vehicles with limited acceleration and deceleration capability reduces the segment capacity. The reason can be found in the spacing-velocity diagram. In Figure 6, the dash line represents the truck (heavy vehicle)-following behaviors. They have larger reaction times compared to passenger vehicles [14]. Hence, Yeo's theory is able to describe the heavy vehicles' impact on the aggregated traffic flow behavior.

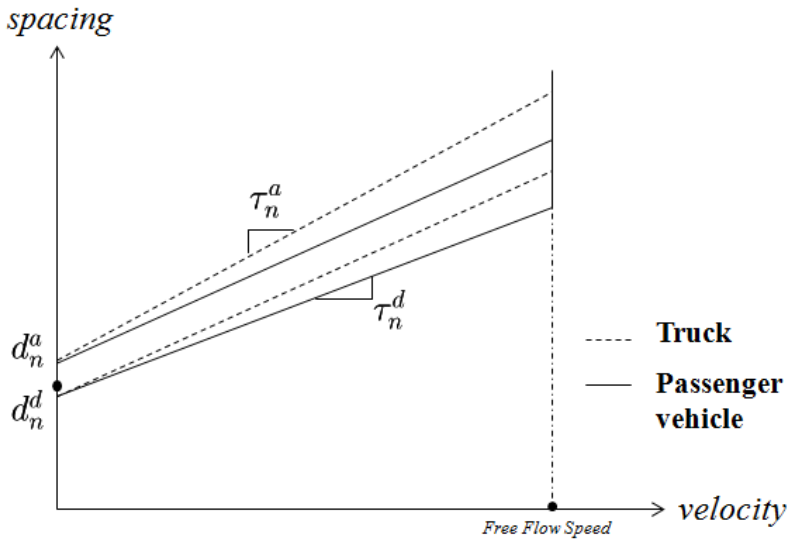

Figure 6 Spacing-velocity relation for different types of vehicles [14]

- ***Mechanism of Shockwave Propagation***

As Figure 7 (a) shows, vehicles A and B have the same spacing-velocity relation and are both traveling at speed v_1; however, the initial following spaces are different. When the leaders change to speed v_2, vehicle A needs to brake as soon as possible, to match the D-curve, which represents a safe driving space between vehicles. Vehicle B has the ability to coast until its spacing reaches the D-curve. Hence, the observed response time for A and B is different [14].

For vehicle A, the time from seeing the leader change speed to completing deceleration is τ_n^d, which is the wave travel time in the time-distance diagram. For vehicle B, the time from seeing the leader change speed until completing deceleration is $\tau_n^d + \Delta s / v_1$, where Δs is the spacing difference between the initial state to the D-curve.

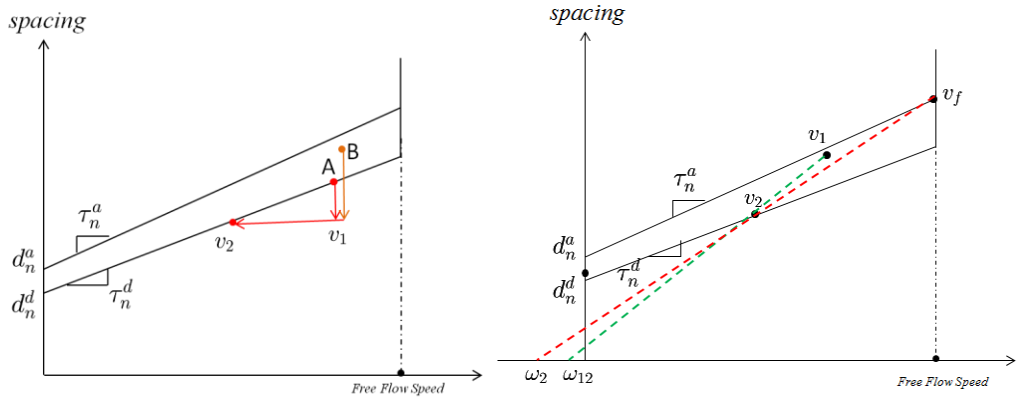

(a) Deceleration process with different spacing (b) Shock wave generated by speed difference

Figure 7 Shockwave in spacing-velocity diagram [14]

Yeo derived the deceleration and acceleration wave speed [14]. As Figure 7 (b) shows, the wave travel time of decelerating from v_1 to v_2 is:

$$\tau_w = \frac{s_2 - s_1}{v_2 - v_1} \tag{3-2}$$

The wave travel distance is:

$$d_n = v_2 \times \tau_w - s_2 \tag{3-3}$$

The shockwave speed is:

$$\omega = \frac{d_n}{\tau_w} = v_2 - s_2 \frac{v_2 - v_1}{s_2 - s_1} \tag{3-4}$$

Therefore, the shockwave speed between these two states is the x-intercept of the line connecting the initial state and the final state [14].

- ***Corresponding Macroscopic Parameters***

Figure 8 shows the relationship between the microscopic parameters and the corresponding macroscopic parameters.

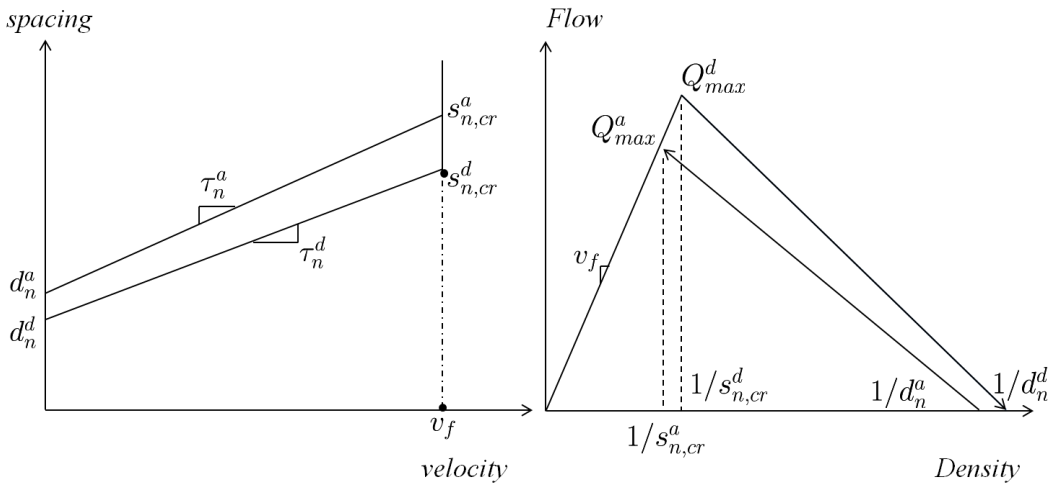

Figure 8 Asymmetric micro- and macro- fundamental diagram [14]

3.1.4 Mathematical Equations of the Extended Car-following Model

To simplify Yeo's car-following equations [14], the authors extended Newell's car-following model in the framework of the asymmetric theory, which can be written as follows:

$$x_n(t+\Delta t) = min\{\underbrace{x_n(t)+u\Delta t}_{freeflow}, \underbrace{x_{n-1}(t+\Delta t-\tau_\omega)-d_\omega}_{congestion}\} \tag{3-5}$$

$$\tau_\omega = \begin{cases} \tau_n^a = \dfrac{s_0 - s^A(v_{n-1})}{v_n - v_{n-1}} & \text{for} \quad acceleration \\ \tau_n^d = \dfrac{s_0 - s^D(v_{n-1})}{v_n - v_{n-1}} & \text{for} \quad deceleration \end{cases} \tag{3-6}$$

$$d_\omega = \begin{cases} d_n^a = v_{n-1}\tau_\omega - s^A(v_{n-1}) & \text{for} \quad acceleration \\ d_n^d = v_{n-1}\tau_\omega - s^D(v_{n-1}) & \text{for} \quad deceleration \end{cases} \tag{3-7}$$

where,

x_n = position of the follower;

x_{n-1} = position of the leader;

τ_w = wave travel time for n^{th} vehicle;

d_w = wave travel distance (jam spacing);

s_o= spacing for n^{th} vehicle before join the wave;

Δt= time step; and

u = free flow speed.

In the above equations, τ_w and d_w depend on the spacing and speed difference once the follower notices the leaders actions. s_0 is located at any point between the A-curve and D-curve, so that τ_w and d_w change dynamically, which captures the dispersion and aggregation of freeway platoons. This asymmetric car-following model was coded in the car-following module.

3.1.5 Mathematical Equations of Car-following Model under VSL control

In VSL-control driving mode, it is assumed that drivers do not sharply decelerate or accelerate upon seeing the current speed limit. Therefore, this study introduces extra parameters in the car-following rule to model the speed limit command impact:

$$x_n(t+\Delta t) = min\{\underbrace{x_n(t)+u\Delta t}_{freeflow}, \underbrace{x_n^*(t+\Delta t)}_{VSL}, \underbrace{x_{n-1}(t+\Delta t-\tau_\omega)-d_\omega}_{congestion}\} \tag{3-8}$$

$$x_n^*(t+\Delta t) = \begin{cases} x_n(t)+\dot{x_n}(t)\Delta t+0.5a_n^\star\Delta t^2 & when \quad t < \dfrac{u_n^\star-\dot{x_n}(t)\Delta t}{a_n^\star} \\ x_n(t)+u_n^\star\Delta t & when \quad t \geqslant \dfrac{u_n^\star-\dot{x_n}(t)\Delta t}{a_n^\star} \end{cases} \tag{3-9}$$

$$\tau_\omega = \begin{cases} \tau_n^a = \dfrac{s_0-s^A(v_{n-1})}{v_n-v_{n-1}} & \text{for} \quad acceleration \\ \tau_n^d = \dfrac{s_0-s^D(v_{n-1})}{v_n-v_{n-1}} & \text{for} \quad deceleration \end{cases} \tag{3-10}$$

$$d_{\omega} = \begin{cases} d_n^a = v_{n-1}\tau_{\omega} - s^A(v_{n-1}) & \text{for} \quad acceleration \\ d_n^d = v_{n-1}\tau_{\omega} - s^D(v_{n-1}) & \text{for} \quad deceleration \end{cases} \tag{3-11}$$

where,

x_n = position of VSL-controlled vehicle *n*;

a_n^* = comfort deceleration/ acceleration rate of vehicle *n*;

u_n^* = desired speed under current speed limit; and

Δt = time step;

3.2 Asymmetric Lane-Changing Model

Modeling the whole process of lane-changing requires the ability to deal with random human manoeuvres. From the literature review, the authors deduce that lane-changing models should have three components: 1) an inducement mechanism for lane-changing; 2) a spatial temporal insertion point generator; and 3) the car-following behaviour after lane-changing.

3.2.1 Modeling Inducement of Lane-Changing

The inducement mechanism falls into two categories: mandatory and discretionary [40]. Laval and Daganzo proposed a lane-changing model to ensure consistency between micro and macro measurements [17]. Similar to [17, 18], we introduce a new term in the lane-changing module, $\tau_{n,LC}$, which is the actual time for vehicle *n* to merge into its target lane.

The mandatory lane-changing occurs at diverge segments. The off-ramp vehicles will change to the adjacent lane of the exit ramp as early as possible. We also selected a critical diverging point for each lane, which means the diverging

vehicles have to change lanes before this location (as shown in Figure 9). The distance of the critical lane-changing point to the exit ramp forced the vehicles to finish lane-changing at the free flow speed. If the diverging vehicle did not finish lane-changing before the critical point, it would stop to wait for a chance to successfully change lanes. The required input for modeling mandatory lane-changing is the number of diverging vehicles and the lane-by-lane distribution of diverging vehicles as they pass the sensor, which requires field observations of driver behaviors. Note that, the diverging location is assumed as a point, rather than an area.

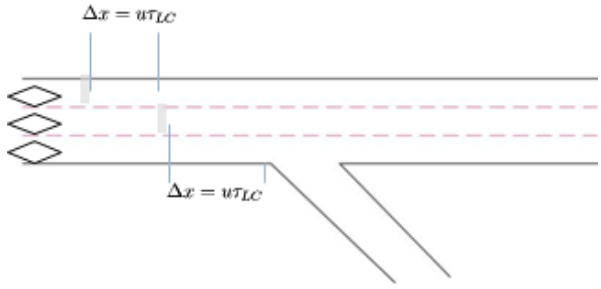

Figure 9 Selection of critical diverge point

Discretionary lane-changing occurs at lane-drop and non-recurrent bottlenecks far away from diverge segments, where the main purpose of lane-changing is to increase the driving speed. Vehicles will move toward the lane that has a higher speed and a lower density.

The principle of Laval's lane-changing model [17, 18, 42]is the demand-supply relation. The method was based on Daganzo's incremental-transfer (IT) principle [18]. The segment was divided into small cells and available capacity was allocated to lane-changing vehicles.

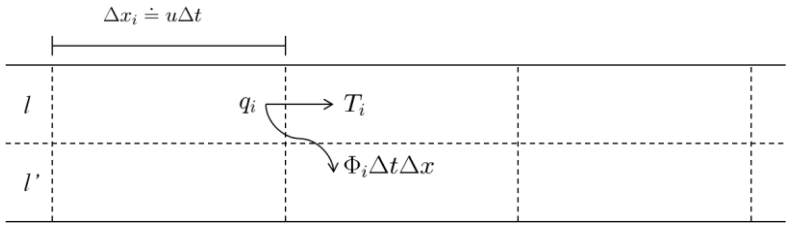

Figure 10 Lane-changing rate in macroscopic framework [17, 18, 42]

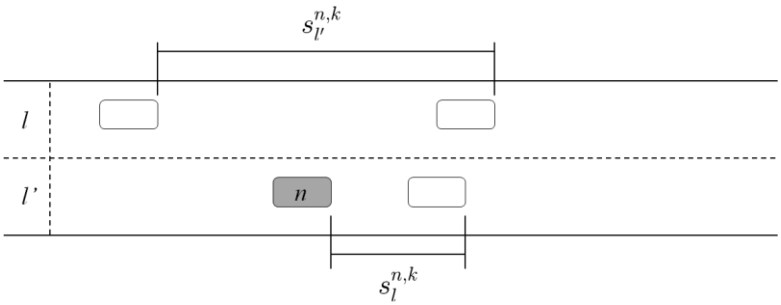

Figure 11 Configuration of lane-changing vehicle in microscopic framework [18]

3.2.2 Generating Spatial Temporal Lane-Changing Point

To model lane-changing in the microscopic framework, Laval derived the probability of vehicle *n* changing its lane from *l* to *l'* at time step *k.* The following equations were validated in previous studies [17, 18].

$$P_{ll'}^{n,k} = \int_{t=k}^{k+1} \int_{x=x_l^{n,k}}^{x_l^{n-1,k}} \Phi(k_l^{x,k}, k_{l'}^{x,k}) dx dt \tag{3-12}$$

$$\Phi(k_l^{x,k}, k_{l'}^{x,k}) = min\{1, \frac{\mu(k_{l'}^{x,k})}{\lambda(k_{l'}^{x,k})}\} \frac{\pi(k_l^{x,k}, k_{l'}^{x,k}) \lambda(k_l^{x,k})}{u} \tag{3-13}$$

$\Phi(\bullet)$ is the net lane-changing rate from lane *l* to *l'* per unit time per unit distance, which is a dependent variable of density at location *x* in time step *k*.

λ is the demand function: $\lambda(k_{l'}^{x,k}) = min\{uk_{l'}^{x,k}, Q_{l'}^{k}\}$ (where, *u* is the free flow speed; $k_{l'}^{x,k}$ is the density at location *x* at time step *k*, which can be approximated as $1/s_{l'}^{n,k}$; $Q_{l'}^{k}$ is the cell capacity from the calibrated FD).

μ is the supply function: $\mu(k_{l'}^{x,k}) = min\{(\kappa - k_{l'}^{x,k})\omega, Q_{l'}^{k}\}$ (κ is the jam density, ω is the maximum shockwave speed)

π is a fraction of drivers per unit time wishing to change lanes from *l* to *l'*, and which varies at different bottlenecks.

$$\pi(k_l^{x,k}, k_{l'}^{x,k}) = \begin{cases} \dfrac{max(v_{l'} - v_l, 0)}{u\tau_{LC}} & \text{discretional} \\ \dfrac{1}{\tau_{LC}} & \text{mandatory} \end{cases} \quad (3\text{-}14)$$

After calculating the lane-changing probability of vehicle *n* via the aforementioned equations, lane-changing is considered as a Bernoulli trial with a success probability of $P_{ll'}^{n,k}$. If the computed trail is successful, then the vehicle will immediately change to the target lane with its current speed.

3.2.3 Modeling the After Lane-Changing Behaviour under Asymmetric Theory

The driving behaviour after lane-changing depends on the incoming spacing. Based on Yeo's observations on NGSIM trajectory data, if incoming spacing is small, then the vehicle must either decelerate or keep its current speed to increase spacing for safety; however, if the spacing is large enough, then relaxation is not required [14]. The relaxation impact can be directly computed from the asymmetric car-following model based on the spacing after lane changing.

3.3 Bottleneck Capacity and Queue Discharge Flow Estimation

3.3.1 The Framework of Bottleneck Capacity Estimation

Figure 12 is the process of bottleneck capacity estimation, which consist of four modules: vehicle entering module, lane-changing module, car-following module and accumulative vehicle count module. The details of functionality of each module is described in the following sections.

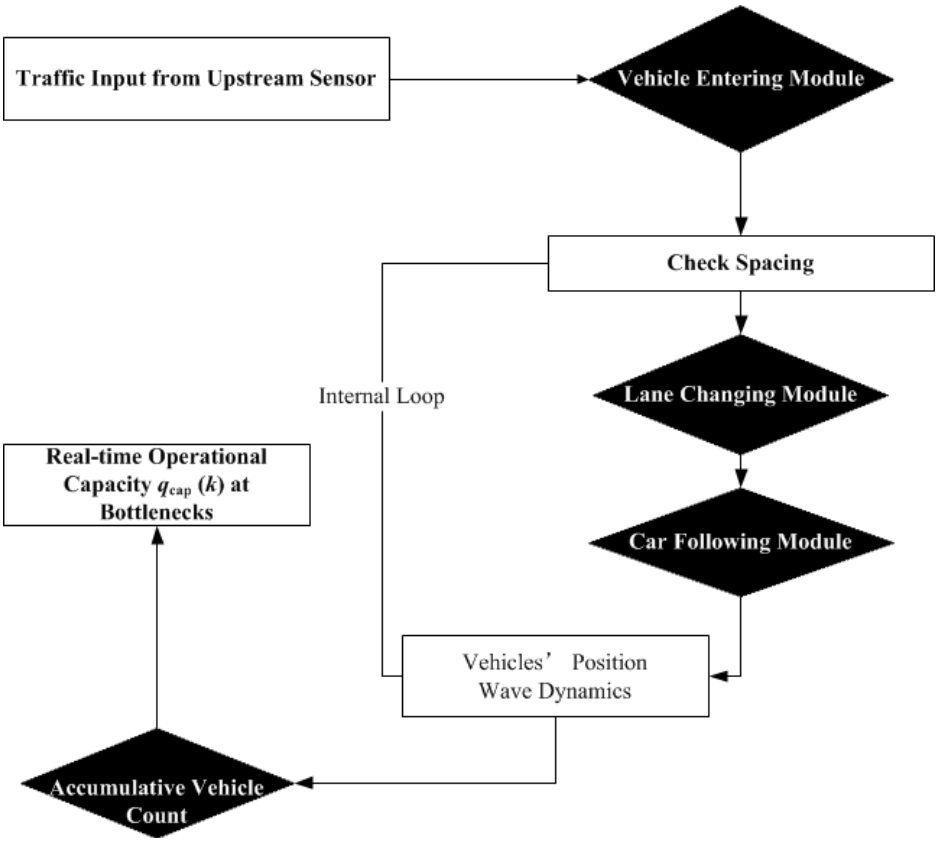

Figure 12 Framework of bottleneck capacity estimation

3.3.2 Vehicle Arriving Assumptions

At the beginning of the simulation, macroscopic lane-by-lane traffic state measurements from upstream sensors were obtained. The vehicle generation algorithm treats the entering vehicle arrival pattern as a Poisson distribution, and the entering speed is assumed homogenous with the desired free flow speed. This study also considered the downstream supply estimated from the last time interval. If the downstream is becoming congested, then the entering vehicle will obey the car-following rule.

3.3.3 Algorithm for Bottleneck Discharge Flow Estimation

This algorithm needs only four parameters from the car-following model and one parameter from the lane-changing model to estimate real-time bottleneck

discharge flow and queue dynamics. Each parameter has physical meaning, and can be estimated from field observations. Once sufficient traffic data sources become available, the parameters can also be extended to represent individual driver's behavior, and more realistic estimations will be generated.

Figure 13 is an illustration of how the flow dynamics at bottleneck locations were obtained: an algorithm that has the same structure as Chen's queue model [37]. After obtaining the front spacing of each vehicle, the algorithm generates the lane-changing point (See Equations 3-12, 13, 14). The shockwave trajectories were constructed by the asymmetric car-following rule, which also considers the relaxation phenomenon after lane-changing. As shown in Figure 13, after lane-changing, if the vehicle has insufficient spacing to accelerate immediately, it will keep either its inserting speed or lower its speed until the spacing increases. This causes a deceleration wave w at D (t_d^w, x_d^w). After the spacing increases, the vehicle will accelerate to the free flow and generate an acceleration wave from D (t_a^w, x_a^w). Note that the wave travel time and wave speed is calculated sequentially from when the first vehicle meets the wave until the wave is dissipated.

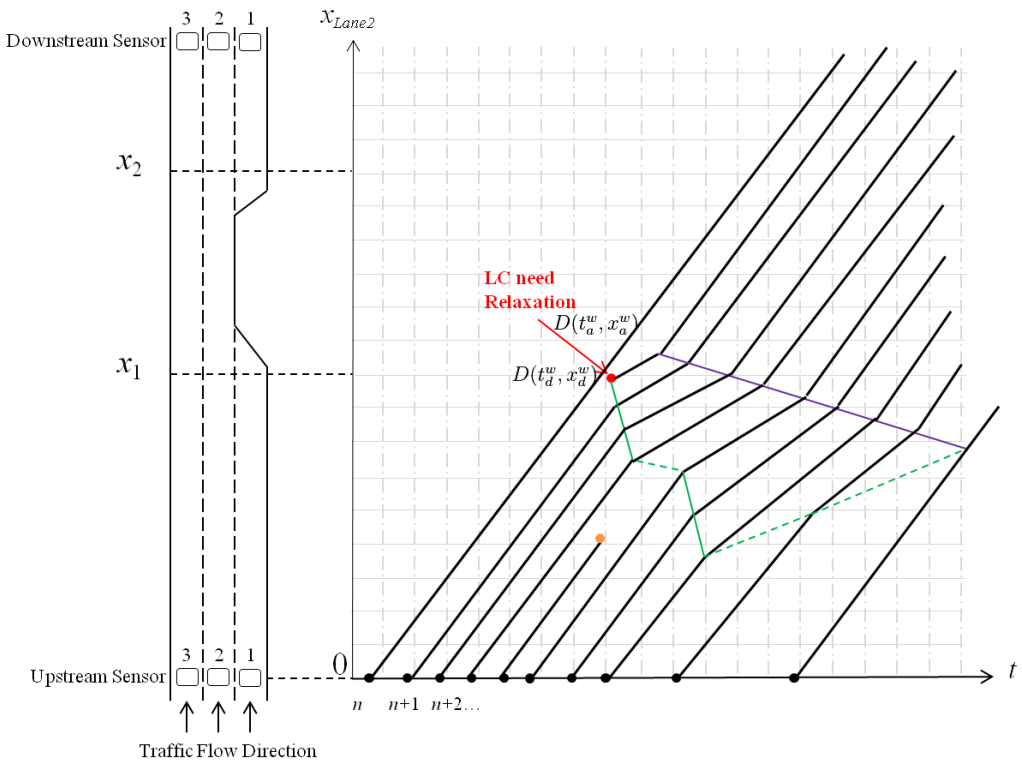

Figure 13 Real-time wave propagation trajectory

For wave *w*, the deceleration point for vehicle *n*+1 is:

$t_{d,n+1}^w = t_d^w + \tau_{d,n+1}, x_{d,n+1}^w = x_d^w - d_{d,n+1}$, the $\tau_{d,n+1}$ and $d_{d,n+1}$ can be calculated from Equations 3-5, 3-6, and 3-7, which require the vehicle *i*+1's initial speed, the spacing when the lane-changing vehicle enters and the entering speed. The corresponding acceleration wave can be computed as the time-space transformation of low speed traffic increasing to free flow speed from the D-curve to A-curve. It was found that the deceleration wave is highly dependent on the incoming vehicle's time or space headway.

The following steps show how to compute the real-time vehicle position and shock wave dynamics at the studied segments:

1. *Setup model parameters*: lane-by-lane car-following behaviors;
2. *Saturated demand*: according to the volume obtained by loop detectors on each lane, determine the merge ratio and the diverge ratio, then give the network saturated demand;
3. *Generate entering vehicles*: the vehicle arrival pattern follows the Poisson distribution. The entering speed is assumed as the free flow speed. The entering headway is larger than the minimum headway: $h_{min} = s_{cr}^{D}/v_f$. The destination of each vehicle is assigned as attribute 0 for through vehicles and attribute 1 for diverge vehicles;
4. *Initialization*: initialize vehicle speed array, vehicle position array, wave speed array and wave position array. If there is a new vehicle entering the lane, add one row to the speed array and position array with its entering speed;
5. *Real-time position*: For existing vehicles on the studied segment, obtain their positioning and spacing at time step *k* (from *k*=1);
6. *Compute lane-changing*: for each vehicle on each lane, compute the lane-changing probability, as shown in Equations 3-12, 3-13, 3-14. Try a Bernoulli trail with a successful rate of $P_{ll'}^{n,k}$; if successful, immediately change lanes and obtain new vehicle positions;
7. *Generate new deceleration wave or acceleration wave*: at time step *k*, compute vehicles' equilibrium spacing (D-curve) lane by lane, for vehicle *n*. If current spacing is smaller than the equilibrium spacing, then the vehicle will decelerate to $v^{D}(s_n)$;

A new deceleration wave *w* is generated at $t_d^w = k$, $x_d^w = x_n^k$. Hence, for vehicle *n*+1, the time it takes to meet the wave is $t_{d,n+1}^w = t_d^w + \tau_{d,n+1}, x_{d,n+1}^w = x_d^w - d_{d,n+1}$, the $\tau_{d,n+1}$ and $d_{d,n+1}$ can be calculated from Equations 3-6, 3-7, which require the vehicle *i*+1's current speed, current spacing, and the vehicle *n*'s current speed. Therefore, wave *w*'s speed is $w_{d,n}^w = d_{d,n} / \tau_{d,n}$.

The acceleration wave can be computed as the time-space transformation of low speed traffic increasing to free flow speed from D-curve to A-curve in Figure 7 (b), which is $t_a^w = t_d^w + \tau_{a,n}^w$. When the vehicle departs from the queue, accelerating from D-curve to free flow speed, the acceleration wave speed will be constant: $w_a^w = v_f - s_{cr}^A \frac{v_f - v^w}{s_{cr}^A - s^D\left(v^w\right)}$;

8. *Compute vehicle position and speed, wave position and speed at next time step k+1*: For vehicle *n*, the position is $x_{n,k+1} = x_{n,k} + v_{n,k}\Delta t$, the speed depends on the upcoming deceleration or acceleration wave. Therefore, compute the wave positions first: $x_{d,n}^w = x_{d,n-1}^w + w_{d,n}^w \Delta t$, $x_{a,n}^w = x_{a,n-1}^w + w_a^w \Delta t$. If $x_{n,k+1} \le x_{d,n}^w$ or $x_{n,k+1} \le x_{a,n}^w$, then the wave will not meet vehicle *n* at time step *k+1*, and the vehicle will keep its current speed. Otherwise, vehicle *n*'s speed at *k*+1 will change to the decreased or free flow speed within the deceleration or acceleration wave;
9. Move to time step k+1, and restart from step 5.

3.3.4 Real-time Capacity Estimation from Discharge Flow Rate

From the aforementioned algorithm, at bottleneck locations, accumulative vehicle counts can be obtained for each time step. To demonstrate the flow characteristics near a bottleneck, the discharge flow, average speed and FD (flow vs. density) near a non-recurrent (lane-drop) bottleneck are shown in Figure 14.

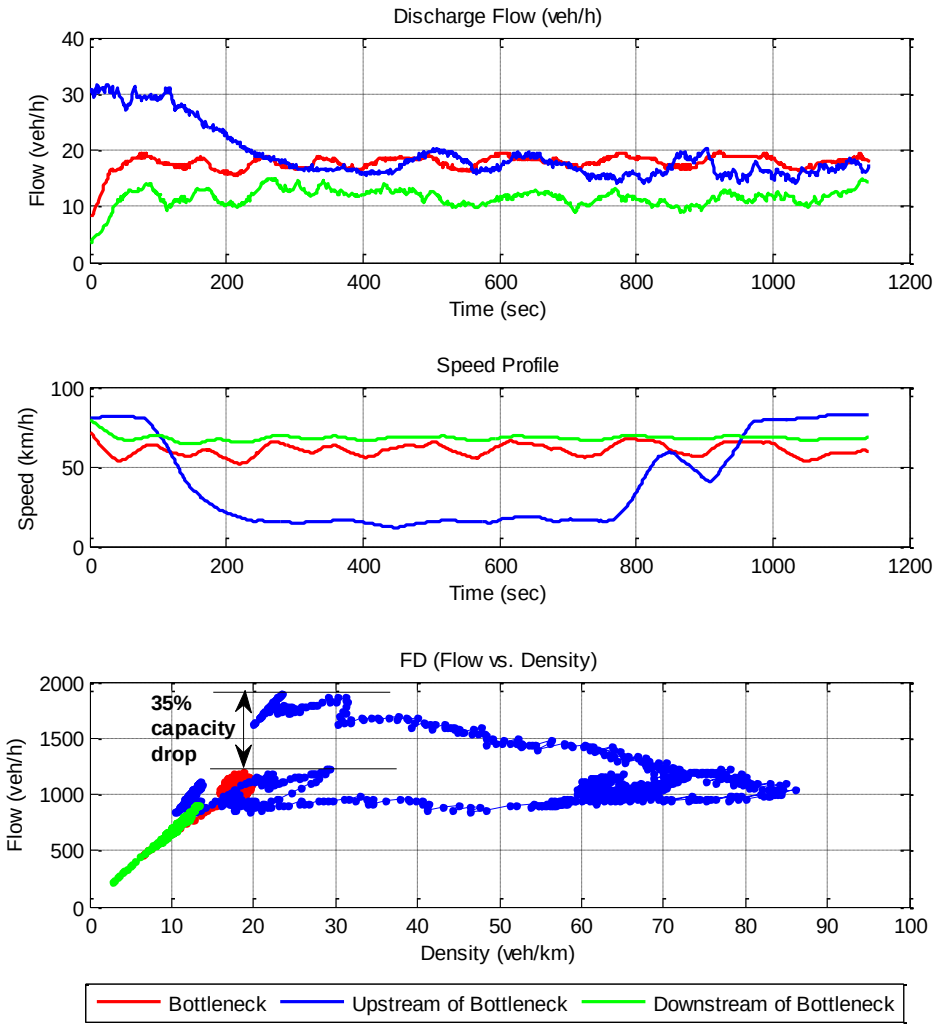

Figure 14 Find bottleneck capacity value

For a homogenous freeway segment, the capacity value should be the same at each measured point. However, the activation of the non-recurrent bottleneck limits the traffic throughput. At the most upstream segment, the flow is

near capacity value before the queue encounters this point. At the bottleneck location, the discharge flow rate is much lower than the capacity value. At the downstream of the bottleneck location, average speed gradually increases to free flow speed. The capacity drop value can be determined as the difference between the maximum discharge flow at the upstream of the bottleneck and the maximum discharge flow at the bottleneck location.

3.4 VSL Operational Capacity and Discharge Flow Estimation

3.4.1 The Framework of VSL Operational Capacity Algorithm

As Figure 15 shows, for a VSL-controlled segment, during the whole simulation period, the basic inputs are measurements from the upstream sensor and the current speed limit. Since the major objective of this study is to determine VSL impact on traffic flow, lane changes in VSL-controlled segments are not considered. Vehicle's real-time position can be obtained based on the proposed asymmetric car-following model. Drivers' compliance to the speed limit change is modeled as different desired speeds and taken from when the driver is able to observe the speed limit change. From the accumulative count, VSLs' real-time operational capacity can be estimated.

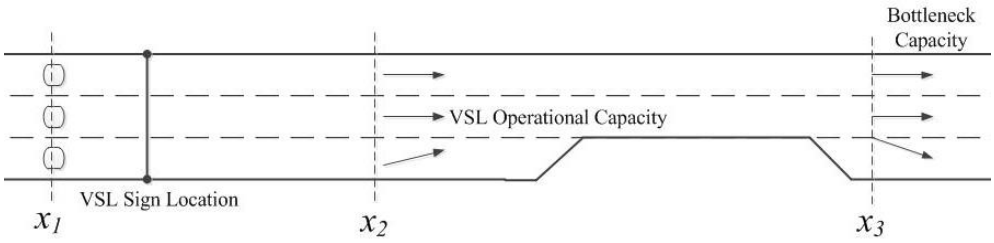

(a) A hypothetical VSL-controlled segment algorithm

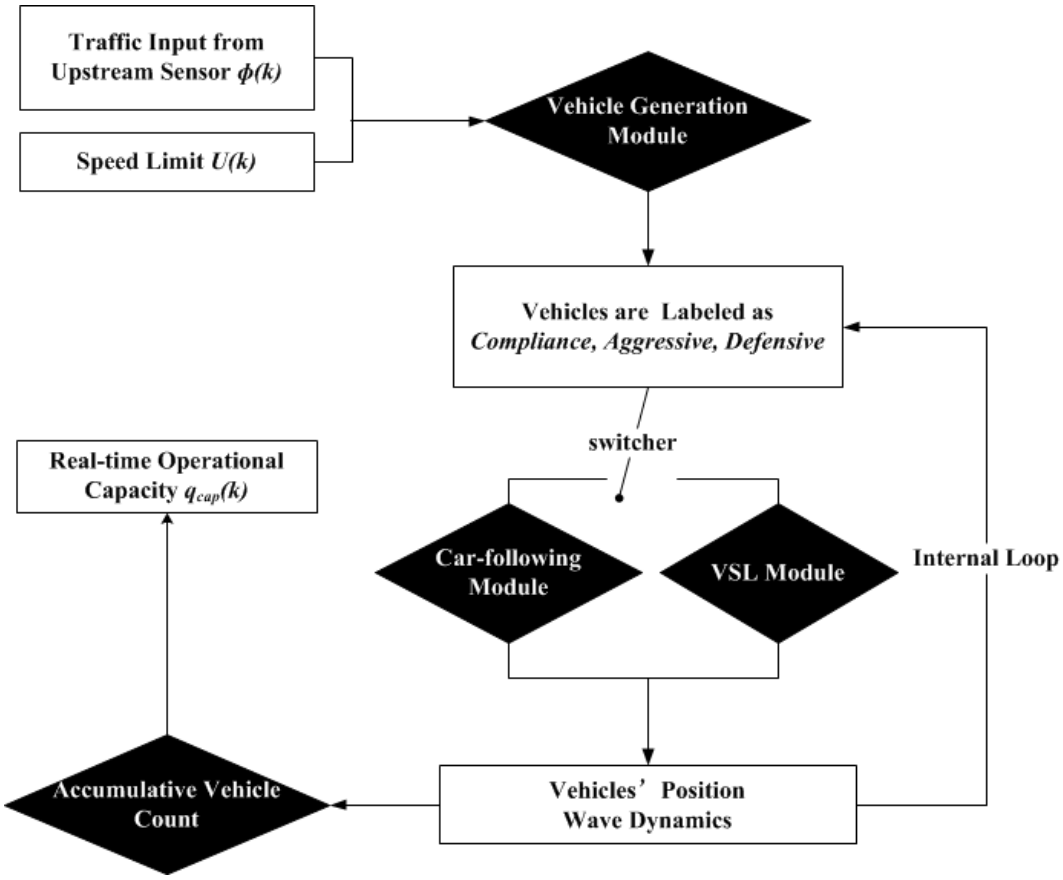

(b) The framework for real-time VSL operational capacity estimation

Figure 15 The framework for the proposed VSL operational capacity estimation

3.4.2 Vehicle Arrival Assumption

At the beginning of the simulation, macroscopic lane-by-lane traffic state measurements from upstream sensors and the current speed limit were obtained. The vehicle arrival was assumed as a Poisson distribution. As well as consider drivers' compliance to the posted speed limit, the vehicle generation module is also able to trigger the desired speed distribution at different speed limits according to the driver compliance level. The simulated drivers were separated into three categories: compliant, defensive and aggressive. The entering vehicles were randomly categorized into one of those three labels. The proportion of each category depends on the compliance level in each speed limit.

3.4.3 Algorithm for VSL-controlled Segment Flow Estimation

This algorithm needs only five parameters from the car-following model (Equations 3-8, 3-9, 3-10, 3-11) to estimate real-time VSL operational capacity. Each parameter has physical meaning, and can be estimated from field observations. Once sufficient traffic data sources become available, the parameters can also be extended to represent individual driver's behavior; therefore, more realistic estimations will be generated.

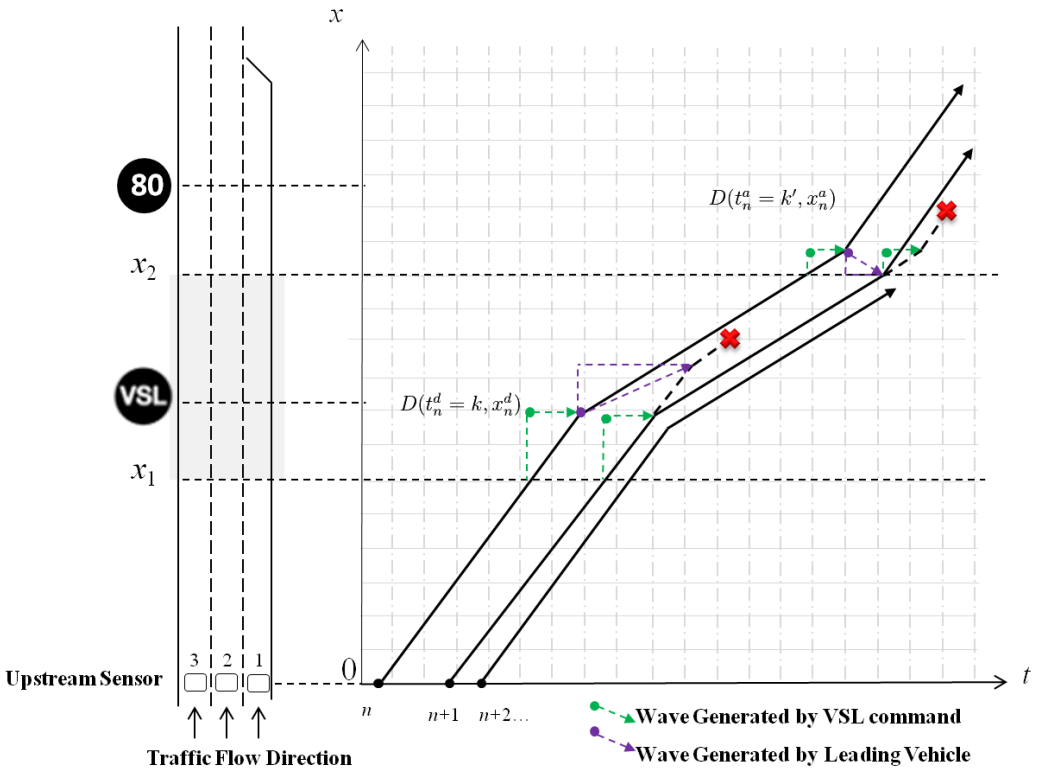

Figure 16 Real-time wave propagation trajectory at VSL-controlled segments

The same as bottleneck capacity estimations, the shockwave trajectories were constructed by using the asymmetric car-following rule. Each vehicle entering and leaving the segment will probably meet two waves. Their speed will change according to the first wave they meet, as Figure 16 shows.

The following steps show how to compute the real-time vehicle position and shock wave dynamics at the studied segments:

1. *Setup model parameters*: lane-by-lane car-following behaviors;
2. *Saturated demand*: give the network saturated demand;
3. *Generate entering vehicles*: the vehicle arrival pattern follows the Poisson distribution, and the entering speed is assumed as the free flow speed. The entering headway is larger than the minimum headway: $h_{min} = s_{cr}^{D}/v_f$;
4. *Initialization*: initialize speed array, position array, wave position array and wave speed array. If there is a new vehicle entering the lane, add one row to the speed array and position array with its entering speed;
5. *Real-time position*: for existing vehicles on the studied segment, get their position and spacing at time step *k* (from *k*=1);
6. *Compute wave travel time and wave speed generated by the VSL command*: at time step *k*, for vehicle *n*, if it just enters the VSL-controlled segment, it will gradually decelerate or accelerate to its desired speed under VSL control. For example, if the posted speed is lower than its traveling speed, a new deceleration wave starts at $t_n^d = k$, and the wave travel time is $t_n^{VSL} = \left(u_n^* - v_n(k)\right)/a_n^*$. Assume that the wave start position is where the vehicle reaches its desired speed u_n^*, $x_n^d = x_n(k) + \left(u_n^{*2} - v_n^2(k)\right)/2a_n^*$; the wave travel distance is then simplified as *0m* (see Figure 16).

   For vehicle *n',* if it just left the VSL-controlled segment x_2, then it will accelerate to the free flow speed as soon as possible. Hence, for vehicle *n* leaving the VSL-controlled segment at time step *k',* a new acceleration

wave starts at $t_n^a = k'$, and the wave travel time is $t_n^{VSL} = \left(v_f - v_n\left(k'\right)\right)\Big/ a_n^*$. Assume that the wave start position is where the vehicle reaches its desired speed v_f , $x_n^a = x_n\left(k\right) + \left(v_f{}^2 - v_n^2\left(k\right)\right)\Big/ 2a_n^*$; the wave speed is then simplified as *0m* and vehicle *n'* will meet the VSL wave when it drives to the wave start position (see Figure 16);

7. *Compute wave travel time and wave travel speed generated by leading vehicles*: the deceleration and acceleration of leading vehicles will also generate deceleration waves and acceleration waves. For example, if vehicle *n* changes its speed at time step *k*, a new wave *w* is generated at $t_d^w = k$, $x_d^w = x_n^k$. The time it takes to meet that wave is $t_{d,n+1}^w = t_d^w + \tau_{d,n+1}, x_{d,n+1}^w = x_d^w - d_{d,n+1}$; the $\tau_{d,n+1}$ and $d_{d,n+1}$ can be calculated from Equations 3-6 and 3-7, which require the vehicle *i*+1's current speed, current spacing, and the vehicle *n*'s current speed. Therefore, wave *w*'s speed is $w_{d,n}^w = d_{d,n} / \tau_{d,n}$.

   Each vehicle will have an acceleration wave caused by the leading vehicle at the point they change their speed to free flow speed v_f , the corresponding acceleration wave speed is $w_a^w = v_f - s_{cr}^A \dfrac{v_f - v^w}{s_{cr}^A - s^D\left(v^w\right)}$;

8. *Compute vehicle position and speed, and wave position and speed at the next time step k+1*: For vehicle *n*, the position is $x_{n,k+1} = x_{n,k} + v_{n,k}\Delta t$, and the speed depends on the deceleration or acceleration wave. Therefore, compute the wave positions first: $x_{d,n}^w = x_{d,n-1}^w + w_{d,n}^w \Delta t$ or

$x_{a,n}^{w} = x_{a,n-1}^{w} + w_a^{w}\Delta t$. If $x_{n,k+1} \le x_{d,n}^{w}$ or $x_{n,k+1} \le x_{a,n}^{w}$, then the wave will not meet vehicle *n* at time step *k+1*, and the vehicle will keep its current speed. Otherwise, vehicle *n*'s speed at *k*+1 will change to the decreased or free flow speed within the deceleration or acceleration wave;

9. Move to time step k+1, and restart from step 5.

3.4.4 Real-Time VSL Operational Capacity Estimation from Discharge Flow

Due to the asymmetric car-following rule, the theoretical VSL operational capacity is deviated, as Figure 17 shows. The capacity at higher speed limits (>=50) does not greatly vary, while lower speed limits (<50) may decrease the freeway efficiency.

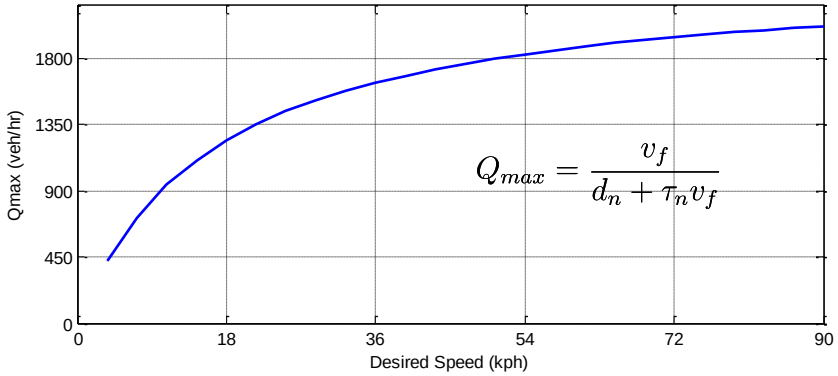

Figure 17 Theoretical VSL operational capacity

From the aforementioned algorithm, at any point of the VSL-controlled segment, accumulative vehicle counts can be obtained in each time step. The maximum discharge flow over 1 minute at the VSL-controlled segment is considered as the operational capacity, as Figure 14 shows.

CHAPTER 4. DATA COLLECTION AND MODEL CALIBRATION

This chapter introduces the study sites, data collection, and model calibration technique as well as the calibration results; then, it presents the experimental design to determine operational capacity in different scenarios. The results and discussions will be presented in the next chapter.

4.1 Studied Site and Field Data

4.1.1 Whitemud Drive in the City of Edmonton

Whitemud Drive (WMD) in the City of Edmonton is an urban freeway with more than 100,000 Annual Average Daily Traffic (AADT). The study corridor is a 7-km section in the westbound direction of WMD between the east of 122 Street (St) and the west of 159 St. Some areas on this freeway stretch are crash-prone locations, which imply a high potential of non-recurrent congestions.

On this study section, two recurrent bottlenecks were identified in previous field studies. The first bottleneck is located on a downstream segment of the 122 St on-ramp, called Terwillegar Drive. Since Terwillegar Drive is a major road that connects highly populated suburban communities with the city's core, diverging demand at Terwillegar Drive off-ramp is always high. In peak hours, when the demand of the 122 St. on-ramp is low, a diverge bottleneck forms a long queue in the leftmost lane. When the demand of 122 St on-ramp is high, the entire segment can be considered a complex weaving segment. The second studied

bottleneck is located downstream of 53 Avenue (Ave). There are two on-ramps at 53 Ave, one is Terwillegar Drive and another connects WMD with 53 Ave. In peak hours, once the on-ramp demand of Terwillegar Drive increases, the segment becomes congested.

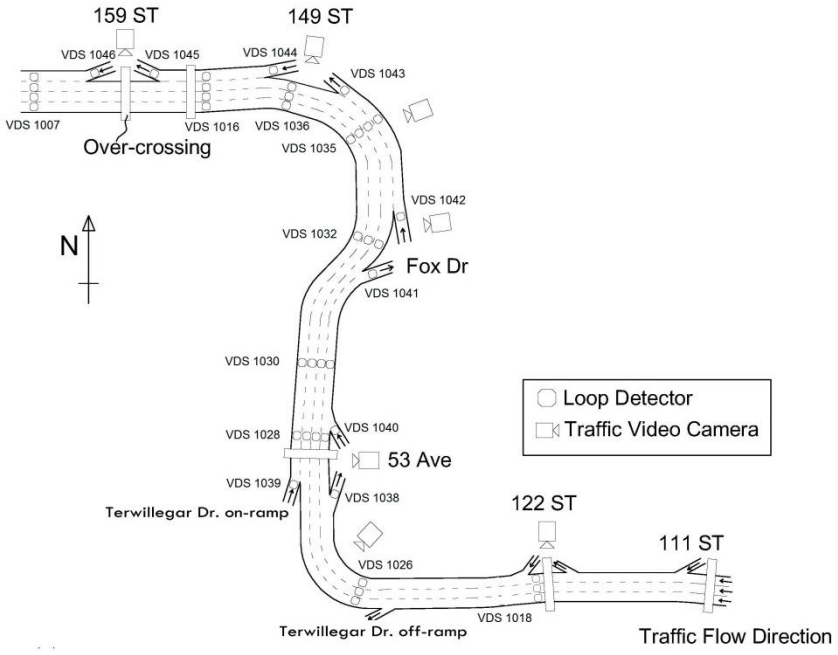

Figure 18 Layout of study corridor

4.1.2 Data Collection

The study corridor is equipped with inductive loop detectors, as Figure 18 shows, the loop detectors send 20-sec field data to a local traffic management center (TMC), which provides traffic states on each link along the whole corridor. The basic input of the proposed algorithm is the real-time traffic origin and destination (OD) at on-ramp and off-ramp locations, which can be roughly measured from the equipped loop detector stations.

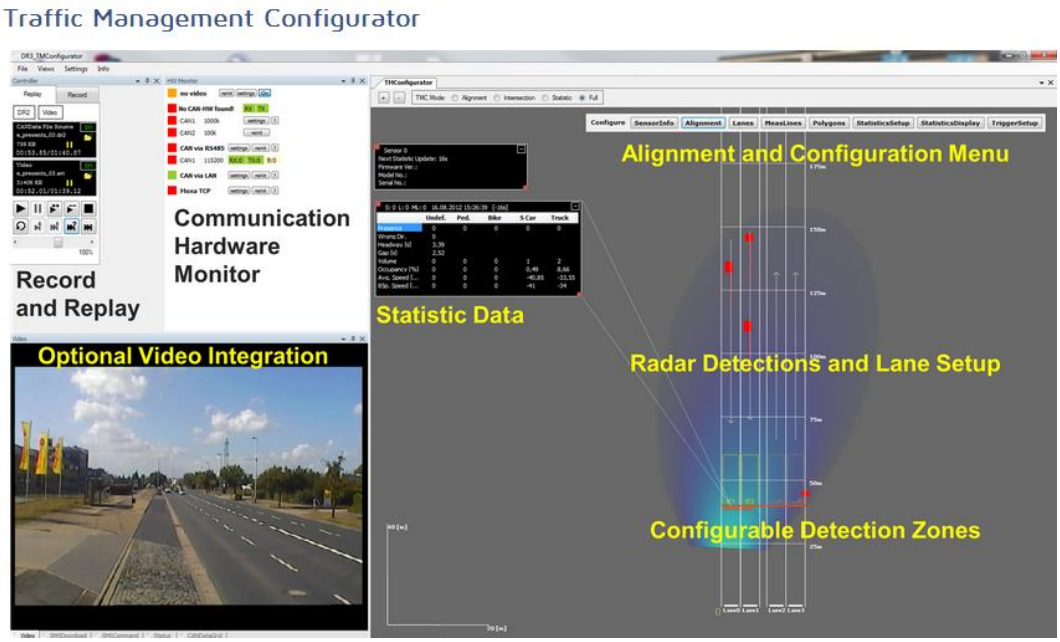

(a) Interface of Smartmicro Traffic Management Configurator [43]

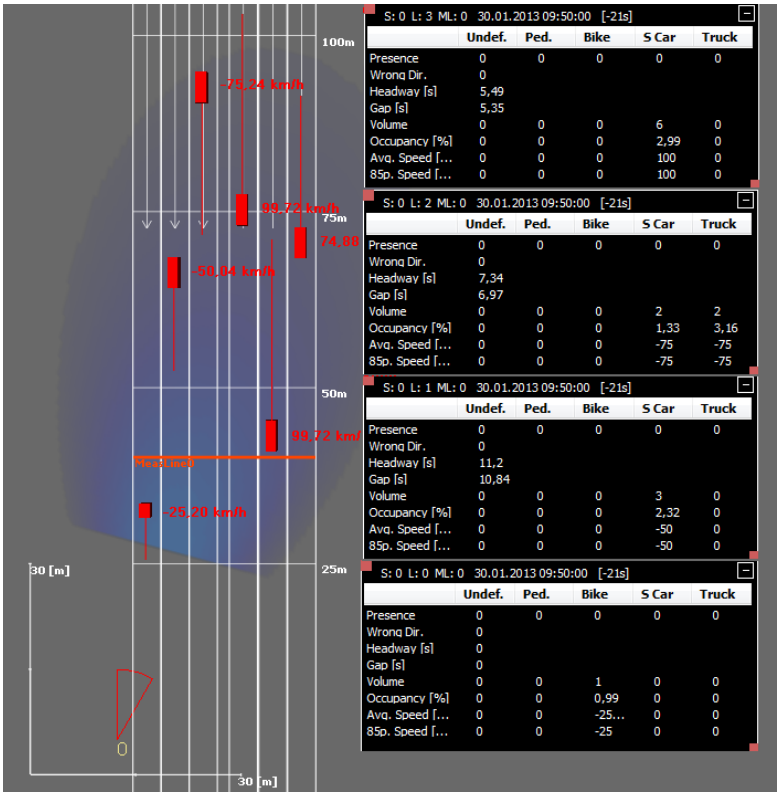

(b) Statistic data interface of Smartmicro Radar Sensor [43]

Figure 19 Smartmicro Traffic Management Configurator Output [43]

To determine the microscopic parameter in the proposed algorithm, this study also used detailed individual vehicle data collected from WMD. Traffic

Radar from Smartmicro was used to detect individual vehicle's presence at the studied segments. The interface of traffic management configurator is shown in Figure 19 (a). Figure 19 (b) shows the interface of statistic data analysis module, four measure lines were placed every 25 meters to obtain lane-by-lane vehicle class, volume, headway and speed every 5 seconds. The detailed headway and speed data for passenger cars was used to calibrate vehicles' average speed-spacing relations, which is the parameter required in the car-following model.

4.2 Model Calibration

4.2.1 Fundamental Diagrams at Studied Segments

From 20-sec loop detector we can get the free flow speed on each lane, which is one of the parameters required for the speed-spacing diagram. Figure 20 is the scatter plot of density-flow relation at bottleneck 1: WMD WB & 122 St. Figure 21 shows the layout of WMD WB & 122 St. Figure 22 is the scatter plot of density-flow relation at bottleneck 2: WMD WB & 53 Ave., while Figure 23 shows the layout of bottleneck 2.

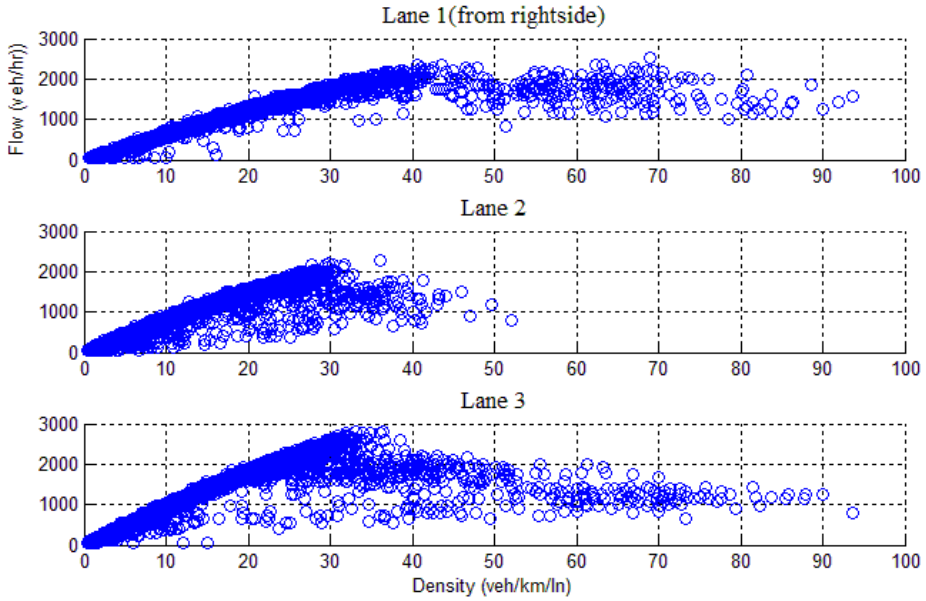

Figure 20 Density-Flow diagram at 122 St (1-min aggregation)

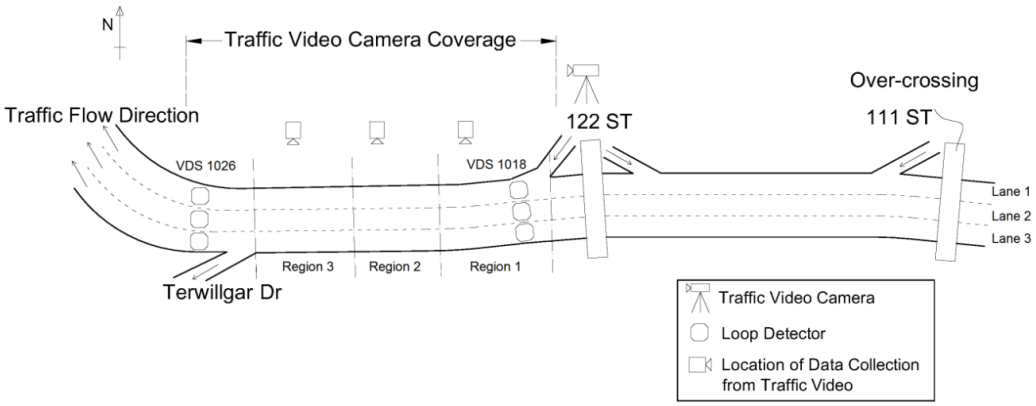

Figure 21 Layout of WMD WB & 122 St Bottleneck

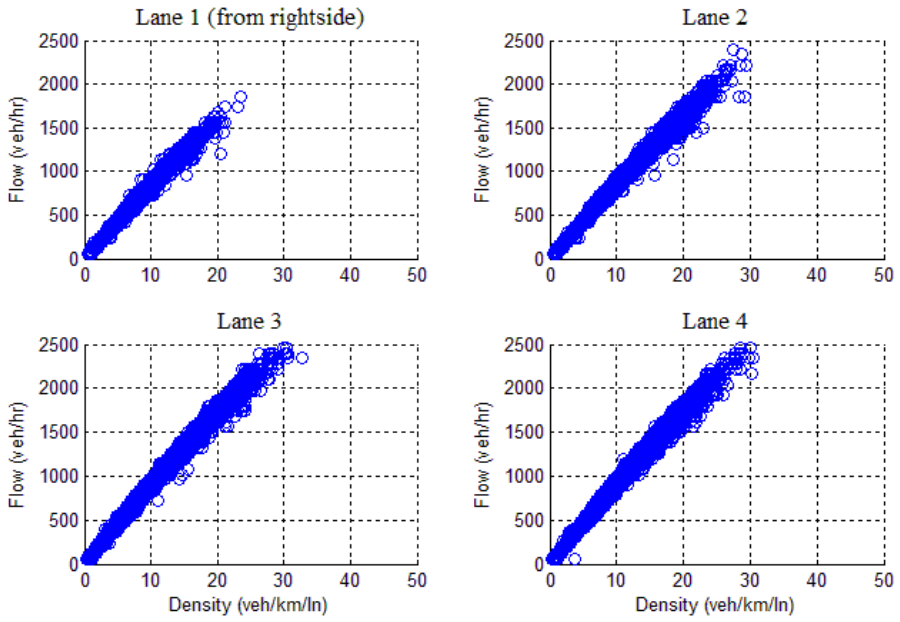

Figure 22 Density-Flow diagram at 53 Ave (1-min aggregation)

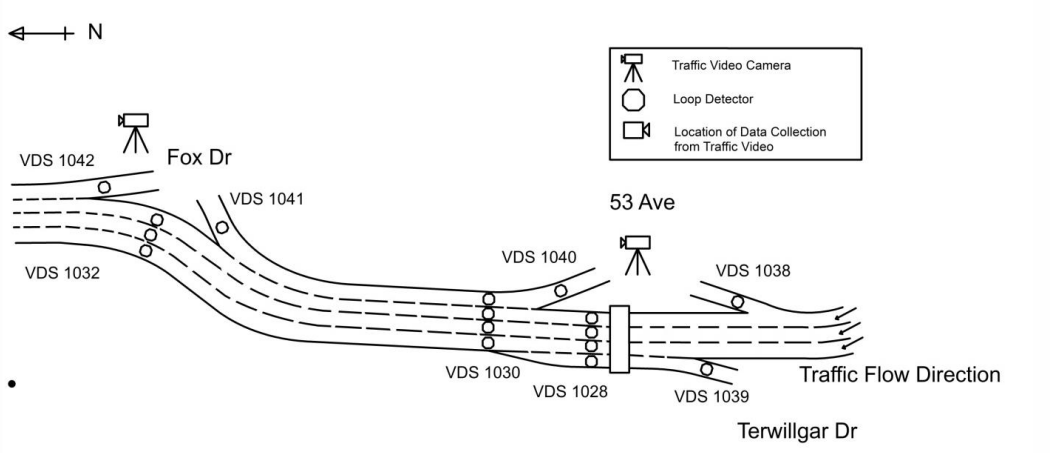

Figure 23 Layout of WMD WB & 53 Ave downstream bottleneck

4.2.2 Microscopic Model Calibration

As stated in the car-following and lane-changing models, there are six parameters to be calibrated: $\tau_n^a, \tau_n^d, s_{jam}^a, s_{jam}^d, \tau_{n,LC}, a_n^*$.

- ***Car-following Model Parameter Calibration***

With the lack of sufficient data sources, individual vehicle's real-time position on the study segment cannot be precisely retrieved. Taken from the radar sensor, the

passenger cars' headway and speed data (taken every 5-sec) was used to calibrate the asymmetric speed-spacing relation.

Since the radar sensor cannot obtain accurate headway and speed data when speed is lower than 10km/h, the passenger cars' stand-still spacing was manually measured from a video recording. As Figure 24 shows, we used two utility poles, which have a distance of 40 m, as reference points to count jam spacing s_{jam}^{a} and s_{jam}^{D}.

If, during one measurement time step (5s) in consecutive measure lanes (25m-distance), the radar sensor reported a speed increase of more than 1.5 metres/second (m/s), then the spacing-speed data was considered to be acceleration. If the reported speed decrease was lower than 1.5m/s, then speed-spacing data was considered to be deceleration. Hence, the actual reaction time is estimated by minimizing the root-mean-square error (RMSE) [44].

$$RMSE = \sqrt{\frac{1}{N}\sum (s_n^{obs.}(v) - s_n^{est.}(v))^2} \qquad [8]$$

where,

N = the number of observed cars in car-following regime;

$s_n^{obs.}(v)$= the observed position of vehicle n at time t;

$s_n^{est.}(v)$ = the estimated position of vehicle n at time t;

Figure 24 Non-recurrent congestion on WMD EB

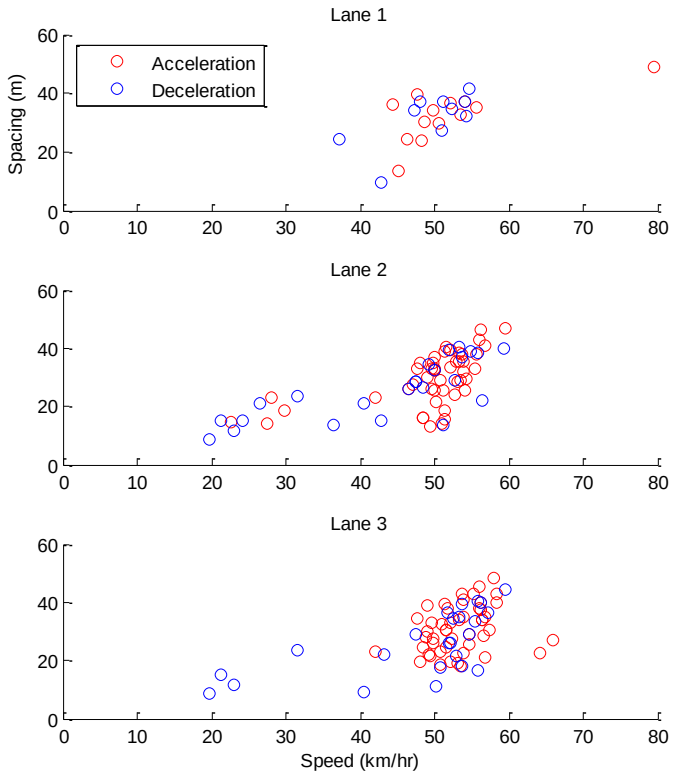

Figure 25 Observed speed-spacing pairs at WMD WB & 122 St

**Total numbers of car-following sample: 176*

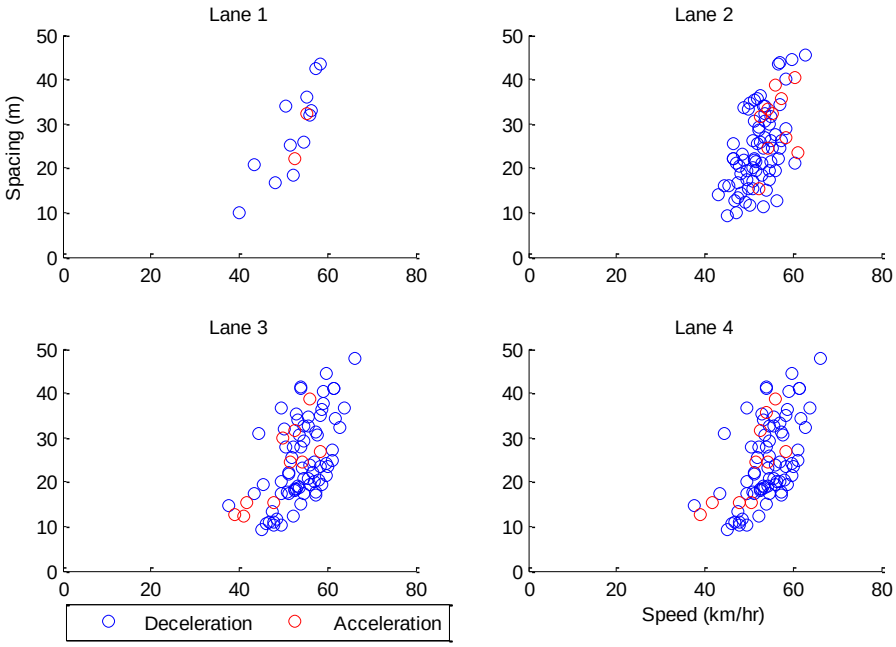

Figure 26 Observed speed-spacing pairs at WMD WB & 53 Ave

**Total numbers of car-following sample: 262*

Table 2 Results of model calibration from field data

Bottleneck 1: Whitemud Dr. WB & 122 St

	Macroscopic parameters		Asymmetric Microscopic parameters			
	Capacity (veh/hr)	Free Flow Speed (km/hr)	τ^a (sec)	d^a (m)	τ^d (sec)	d^d (m)
Lane 1	2520	82	1.78	7.9	1.68	6.3
Lane 2	2760	82	1.73	7.9	1.54	6.3
Lane 3	2820	90	1.68	7.9	1.41	6.3

Bottleneck 2: Whitemud Dr. WB & 53 Ave

	Macroscopic parameters		Asymmetric Microscopic parameters			
	Capacity (veh/hr)	Free Flow Speed (km/hr)	τ^a (sec)	d^a (m)	τ^d (sec)	d^d (m)
Lane 2	2400	85	1.43	7.9	1.25	6.3
Lane 3	3000	88	1.28	7.9	1.26	6.3
Lane 4	2940	92	1.30	7.9	1.25	6.3

** The parameters on lane 1 are assumed the same as those on lane 2*

- ***Lane-Changing Parameter***

For the lane-changing parameter $\tau_{n,LC}$, the video recorded from cameras on the WMD was used for data observation and collection. The total time for a vehicle to move to the target lane is 3-4 sec. Hence, based on recommendations from a previous study [17, 18], an approximated value of the lane-changing parameter is $\tau_{n,LC} = 4\text{sec}$, in this study.

- ***Selection of Comfortable Deceleration or Acceleration Rate***

A comfortable acceleration and deceleration rate $a_n^{\star}$ was assumed to be 2.5m/s^2. Further studies will examine the sensitivity of drivers' comfortable acceleration and deceleration rates.

CHAPTER 5. RESULTS AND DISCUSSIONS

This chapter presents the capacity estimation results. For each type of studied freeway segment, the capacity was influenced by several determining factors. Therefore, experiments were designed to qualify those factorial impacts.

5.1 Principle of Experiment Design for Capacity Estimation

As stated in the algorithm section, the operational capacity at complex freeway segments is influenced by the traffic demand. From the basic input, for example, the merging ratio, diverging ratio, and lane drop location, it is understood that 1) the determining factor of bottleneck capacity is the lane-changing frequency, which is a result of traffic OD at the studied segment; and 2) the determining factor of a VSL segment is the drivers' response to the VSL command. Note that to obtain capacity value, the saturated flow rate should be set to the algorithm. If using the real-world traffic demand at the upstream sensor, the output of this algorithm is the real-time discharge flow at the studied segment.

5.2 Capacity Estimation at Non-Recurrent and Lane-Drop Bottlenecks

For a lane-drop or an unplanned incident-caused non-recurrent bottleneck, this algorithm needs only the incident location to address the magnitude of the capacity drop. At the reverse direction (WMD EB & 122 St.) of study site one (WMD WB & 122 St.), an incident occurred on July 24. During the first hour

after the incident occurred, two lanes of traffic were blocked. After the first hour, one of the blocked lanes was cleared. Capacity drop in different scenarios was obtained by taking the loop detector data measurements from the July 24 incident as the ground truth, using the parameters at WMD WB &122 St, giving the saturated demand and by blocking different lanes. Table 3 lists the results of the non-recurrent (lane-drop) bottleneck capacity estimation.

Table 3 Results of lane-drop bottleneck capacity estimation

	Incident Location	Incident Lane-block	Base Capacity (veh/h/ln)	Bottleneck Capacity (veh/h/ln)	Capacity Drop	Capacity Drop in HCM	Observed Maximum Discharge Flow* (veh/h/ln)
1	lane 1	1-lane-block	1860	1200	35%	51%	1084(41%)
2	lane 2	1-lane-block	1860	1100	41%		---
3	lane 3	1-lane-block	1860	1160	38%		---
4	lane 1 & 2	2-lane-block	1860	680	63%	83%	610 (67%)
5	lane 2 & 3	2-lane-block	1860	700	62%		---

** The field data was collected from loop detectors located 300m upstream of the non-recurrent bottleneck and the bottleneck capacity was measured as the maximum discharge flow in 15 min.*

The results show that the proposed method gives more accurate estimations compared to the capacity drop values suggested by HCM. The magnitude of the capacity drop varies in different scenarios. As the results show, a one-lane block at the study site can cause a capacity drop of 35-41%, while a two-lane block may cause a 62-63% capacity drop. For real-time bottleneck capacity estimation, as long as the incident location is known, the capacity of the activated non-recurrent bottleneck can be estimated.

5.3 Capacity Estimation at Merging Bottlenecks

For a merge bottleneck, this algorithm needs only the merging and main lane demand. This section presents the results of capacity estimation for study site two, (WMD WB and 53 Ave [Terwillegar Drive], as Figure 23 shows).

- ***Impact of Merging Ratio***

For the studied segment, WMD WB & 53 Ave., give the segment saturated demand with the different merge ratio; then, capacity drop in the different scenario will be obtained.

Table 4 Capacity at Merge Bottleneck with Different On-ramp Demand

scenario	53Ave. On-ramp Demand (veh/h/ln)	Terwilleger Dr. Demand (veh/h/ln)	Main lane Demand (veh/h/ln)	Measured Capacity (veh/h/ln)	Bottleneck Capacity (veh/h/ln)	Capacity Drop (%)
1	800	2000	2200	2145	1800	16%
2	1200	2000	2200	2145	1800	16%
3	1600	2000	2200	2145	1800	16%
4	2000	2000	2200	2145	1800	16%
5	2000	1600	2200	2145	1995	7%
6	2000	1200	2200	2145	2010	6%
7	2000	800	2200	2145	2040	5%

As shown in Table 4, the maximum capacity drop is approximately 16%. Scenarios 1-4 test the impact of the 53-Ave on-ramp demand, along with the saturated demand on Terwillegar Drive, where the capacity drop is always 16%, which means that the 53 Ave on-ramp traffic flow does not influence traffic efficiency at this location. Scenarios 4-7 test the impact of the Terwillegar Drive merging demand. When the merging demand decreases, the magnitude of the capacity drop decreases. The results show that at the studied location, the capacity drop is caused only by the merging flow from Terwillegar Drive. One possible

reason is that, in this algorithm, merging is assumed to occur at a particular point. The geometry features (see Figure 23) determine the traffic stream from the Terwillegar on-ramp merging into the main lane. Meanwhile, the 53 Ave on-ramp flow can directly travel to the main lane without changing lanes.

- ***Impact of Main Lane Volume***

The impact of the main lane volume is analyzed by changing the main-stream volume. When the upstream demand decreases, the magnitude of the capacity drop decreases, because there is more space for Terwillegar Drive on-ramp vehicles merging into the main-stream, requiring less frequent decelerations and accelerations.

Table 5 Capacity at merge bottleneck with different main lane demand

scenario	53Ave. On-ramp Demand (veh/h/ln)	Terwilleger Dr. Demand (veh/h/ln)	Main lane Demand (veh/h/ln)	Measured Capacity (veh/h/ln)	Bottleneck Capacity (veh/h/ln)	Capacity Drop (%)
8	2000	2000	2000	2145	1905	11%
9	2000	2000	1800	2145	1920	10%
10	2000	2000	1600	2145	1980	8%

5.4 Capacity Estimation at Diverging Bottlenecks

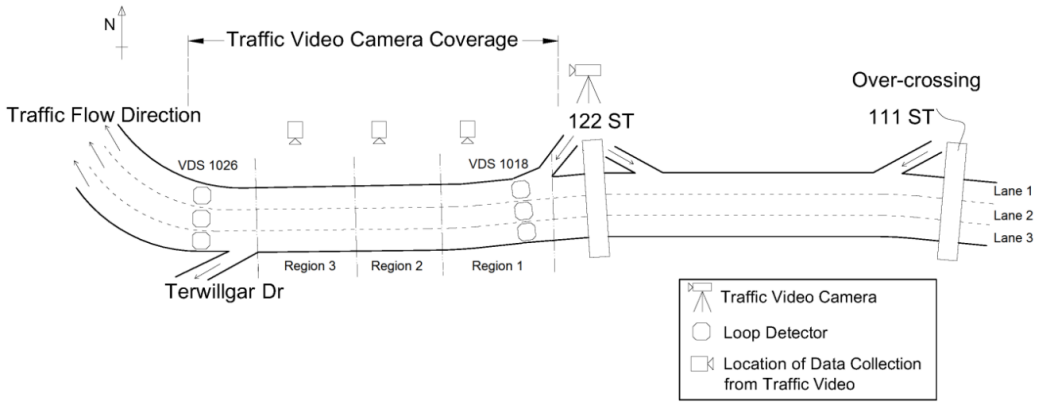

Figure 27 Video recording and layout of WMD WB & 122 St bottleneck

For the studied diverging bottleneck, this algorithm needs only the diverging ratio and proportion of diverging vehicles in each lane. The real-time proportion of diverging vehicles on each lane is difficult to measure. Hence, in this study, video data counts for one day during peak hours were used. As shown in the video observation, 30% of the upstream demand (main-stream plus on-ramp) took the Terwillegar Drive off-ramp. The video shows that Region 1 in Figure 21 is the critical lane changing region. The algorithm considers this observation by assuming lane-changing vehicles move to the target lane as early as possible. The proportion of diverging vehicles on lane 1 to lane 3 are assumed as 1/2, 1/3 and 1/6, based on the video observations.

For real-time diverging bottleneck capacity estimation, an accurate diverging ratio is difficult to measure, even when the off-ramp is equipped with loop detectors. Taking the previous 5-10 min diverging ratio is recommended. Table 6 shows the estimated bottleneck capacity when the ratio of diverging

demand over the main lane demand increases. The capacity drop ranges from 3-16% when the diverging demand increases.

Table 6 Results of diverging bottleneck capacity estimation

scenario	Terwilleger Dr. Diverge (veh/h/ln)	Main lane Demand (veh/h/ln)	Diverging demand / main lane demand	Measured Capacity (veh/h/ln)	Bottleneck Capacity (veh/h/ln)	Capacity Drop (%)
1	1200	2000	0.2	1820	1760	3%
2	1800	2000	0.3	1820	1700	7%
3	2400	2000	0.4	1820	1520	16%

5.5 Capacity Estimation at VSL-controlled Segments

- ***Impact of Drivers' Compliance***

According to a recent study [45], compliance level was categorized as "low, moderate, high, and ideal". In that study, field loop detector data (taken over a 2-month period), was analyzed, by a commercial software, named TOPS, for the local drivers' compliance to a speed limit of 80km/h. Based on that statistical analysis, drivers' compliance levels under different speed limits were modeled. For example, the desired speed distribution for a 60 km/h VSL command with low compliance was modeled, as Figure 28 shows. Table 7 shows the results and the assumed compliance levels at different speed limits [45].

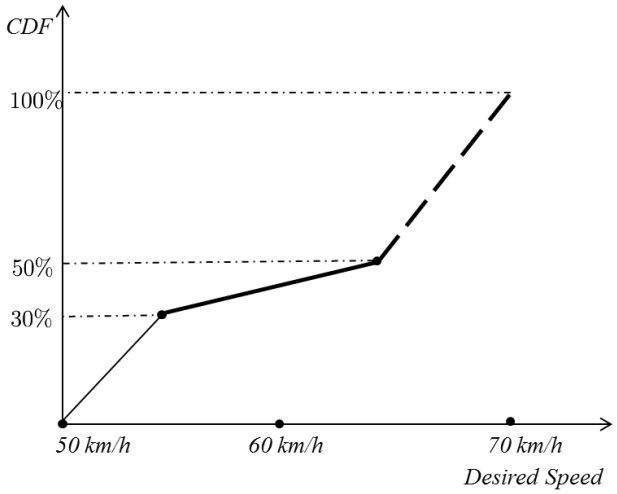

Figure 28 Linear approximation of desired speed distribution

Table 7 Assumption of compliance levels in different speed limits [45]

VSL/ kph	Compliance Levels (%)			
	low		ideal	
	defensive	aggressive	defensive	aggressive
20	30	50	0	0
30	30	50	0	0
40	30	50	0	0
50	30	50	0	0
60	40	40	0	0
70	40	40	0	0
80	40	40	0	0

This study uses the same compliance level assumption as [45]. With the assumed distribution of drivers' compliance, the desired speed is randomly distributed to the vehicles. With their desired speed, vehicles' speed and position at the VSL-controlled segment is computed with the proposed algorithm. Table 8 shows the results of VSL operational capacity estimation considering "low" driver compliance. The estimated operational capacity in "low" compliance is slightly lower than that of an "ideal" situation. The reason is that in "low" compliance, defensive drivers' desired speed at the posted speed limit is lower than the VSL

command, which constrains the following vehicles; hence, the estimated capacity is lower than "ideal".

Table 8 VSL operational capacity estimation considering driver compliance

VSL Operational Capacity (veh/h/ln)	20 km/h	30 km/h	40 km/h	50 km/h	60 km/h	70 km/h
Ideal	1320	1590	1680	1720	1800	1780
Low	1240	1480	1580	1680	1740	1760

- ***Transition Flow among Different Speed Limits***

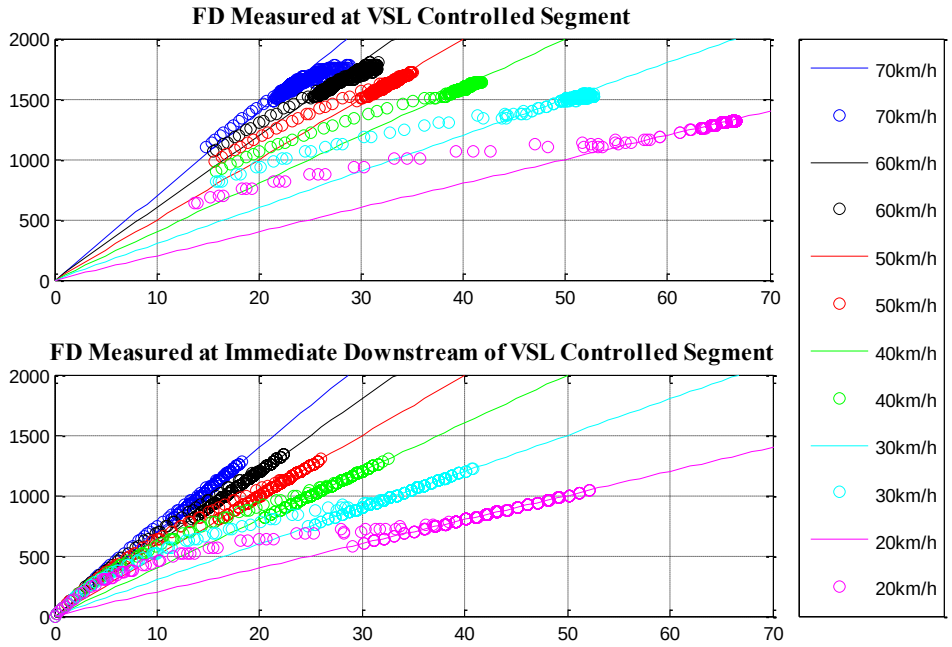

Figure 29 Fundamental Diagram (density vs. flow) at VSL-controlled segment

With the assumption that vehicles will gradually change their speed to the posted speed limit within a comfortable acceleration or deceleration rate, it is obvious that the whole traffic stream will gradually change speed to the posted speed limit. As Figure 29 shows, the upper FD is measured from the midpoint of the VSL-controlled segment. It is clear that the lowered speed limits gradually

increased the segment density. Speed limits set at 60 km/h and 70 km/h maintain the freeway capacity and increase critical density. At the downstream of the VSL-controlled segment, traffic streams accelerate to the free flow speed to pass the bottleneck as quickly as possible. This transition flow effect can be observed in the FD: the density decreases, while the average speed gradually increases to the free flow speed. These results are consistent with the VSL field study conducted by Papagergiou et al. [19], which was a comprehensive field study on the flow impact of VSL. They found that by decreasing speed limits, the average speed at under-critical occupancy also decreased, while the critical density increased.

CHAPTER 6. CONCLUSIONS AND RECOMMENDATIONS

This chapter presents the major findings and contributions of this study. The proposed method also has some limitations, which are summarized after the conclusions. From this comprehensive study of capacity at complex freeway segments, this chapter puts forward some thoughts and recommendations for future works.

6.1 Conclusions

6.1.1 Research Summary

Bottlenecks and VSL-controlled segments are critical locations for freeway operations. Acceleration, deceleration and lane-changing caused by roadway geometric features and VSL commands are considered to be the main factors influencing segment capacity. Considering the microscopic traffic models' flexibility in capturing the flow dynamics at complex freeway segments, this study uses the car-following and lane-changing models to mathematically describe driving behaviour at complex freeway segments.

Asymmetric driving behaviour was employed as the framework of the microscopic traffic models. The principle of the Asymmetric Theory is that drivers are used to having a larger headway when accelerating compared to when decelerating, given the same speed. The Asymmetric Theory was developed in 1965; however, few analytical models describe this phenomenon. In 2008, Yeo

proposed an asymmetric driving behaviour theory and validated his arguments by NGSIM trajectory data [14]; however, Yeo did not perform a qualitative analysis of the theory. This thesis fills that gap by developing the car-following and lane-changing models under the Asymmetric Theory, and assessing the model performance with field data collected from Whitemud Drive in the city of Edmonton.

Simplified lane-changing and car-following models were developed under the framework of asymmetric driving behavior. The models were extended from a base lane-changing model [17] and a car-following model [29], which are well-known benchmarks in freeway traffic flow research. Compared to the base car-following model, the proposed model using asymmetric behaviour addresses the disturbance caused by acceleration and deceleration. Compared to the original lane-changing model [17] and its later version [18], the proposed model using asymmetric behaviour more realistically reveals the relaxation phenomenon after lane changing.

After extending the lane-changing and car-following models to an asymmetric framework, this study developed algorithms to obtain real-time wave position and vehicle positions at critical freeway segments. The proposed algorithm is an extension of the microscopic queue model proposed by Chen et al. [37]. Chen's queue model considered only vehicles' asymmetric longitudinal behaviours, while the acceleration time for vehicles passing the bottleneck was assumed to be fixed. This paper moved beyond that by considering the lane-

changing impact. Moreover, acceleration and deceleration behaviours were calculated from mathematical equations.

By modeling the wave propagation considering the lane-changing impact, this paper estimates real-time discharge flow under the framework of asymmetric driving behaviour in congested traffic. The freeway operational capacity at critical segments is obtained as the maximum discharge flow rate. The estimation results are consistent with similar studies [8, 17, 18].

6.1.2 Research Findings

From field observations and results analysis, there are two major findings of this study:

- Lane-changing is a major contributor to capacity drop at freeway bottlenecks. Take the WMD WB & 122 St diverge ramp for example: frequent lane-changing manoeuvres occur at this location; many vehicles need to change to the leftmost lane to take the exit ramp. When the diverging demand is high, frequent lane changing causes traffic breakdowns and huge capacity drops. Another on-ramp bottleneck example is WMD WB & 53 Ave; vehicles from this on-ramp do not need to change their travelling lane. Here, the capacity drop is caused only by the merging behaviour from the upstream Terwillegar Drive on-ramp.
- Freeway operational capacity under VSL control is also discussed Decreasing speed limits increases critical density. The operational capacity under higher speed limits (>=50 km/h) does not significantly vary; however, lower speed limits (<50 km/h) may decrease freeway efficiency.

In this situation, VSL may improve only traffic safety, rather than traffic flow.

6.1.3 Limitations of the Research

This research has some limitations. It lacks sufficient field data to capture individual vehicle's behaviour. Hence, this study uses one set of car-following model parameters to represent the whole traffic stream, which is not valid from a microscopic point of view. This study also uses arbitrarily selected model parameter values, such as the lane-changing parameter and the comfortable acceleration or deceleration rate at VSL segments, suggested by a previous study. However, since the main purpose of this study is to estimate discharge flow and capacity, the parameters represent the average driving behaviour on WMD, which does not have significant influence on the accuracy of macroscopic measurements.

Another limitation is that complex geometry features are sometimes simplified. For example, at merging and diverging bottlenecks, this study assumes that the vehicles are exiting or entering the freeway at a certain point; the acceleration area at ramps is not considered. Also, this study assumes that there are no slopes on the studied segment.

6.2 Future Work and Recommendations

From the field study and research analysis, there are three major suggestions and recommendations for traffic demand management strategies:

- In the wave propagation algorithm, there is an indication that upstream demand is a key factor in congestion wave expansion. If active traffic

control strategies, such as Ramp Metering and Variable Speed Limit, can smooth the upstream demand, and provide sufficient spacing for lane-changing traffic streams, the probability of breakdown from small local oscillations will be reduced;

- Heavy vehicles are a critical component of freeway operation. Although heavy vehicles were not computed in the algorithm for discharge flow estimation, from field data collection, it was found that the time for trucks to change lanes or accelerate to free flow speed is much higher than the time it takes for passenger cars to complete the same tasks. The free flow speed of trucks is lower than that of passenger cars. Hence, managing heavy vehicles' lane-changing activities may potentially increase bottleneck capacity.
- The proposed algorithms will have better performance when individual vehicle data is available. Advanced technologies and methodologies for data collection and analysis of individual vehicle behaviours are needed.

REFERENCES

[1] M. Hadiuzzaman, T. Z. Qiu and X. Lu, "Variable Speed Limit Control Design for Relieving Congestion Caused by Active Bottleneck," *ASCE Journal of Transportation Engineering*, vol. 139, no. 4, pp. 358-370, 2013.

[2] M. Papageorgiou, J.-M. Blosseville and H. Hadj-Salem, "Modelling and real-time control of traffic flow on the southern part of Boulevard Peripherique in Paris: Part I: Modelling," *Transportation Research Part A: General*, vol. 24, no. 5, pp. 345-359, September 1990.

[3] M. Papageorgiou, J.-M. Blosseville and H. Hadj-Salem, "Macroscopic modelling of traffic flow on the Boulevard Périphérique in Paris," *Transportation Research Part B: Methodological*, vol. 23, no. 1, pp. 29-47, February 1989.

[4] M. M. Michiel, B. Hein and B. H. Piet, "Assessment of Roadway Capacity Estimation Methods," *Transportation Research Record: Journal of the Transportation Research Board*, vol. 1572, no. 1, pp. 59-67, January 1997.

[5] L. Leclercq, J. A. Laval and N. Chiabaut, "Capacity Drops at Merges: an endogenous model," in *19th International Symposium on Transportation and Traffic Theory*, Berkeley, CA, 2011.

[6] A. Hegyi, B. De Schutter and J. Hellendoorn, "Optimal coordination of

variable speed limits to suppress shock waves," *Proceeding of IEEE Transactions on Intelligent Transportation Systems,* vol. 6, no. 1, pp. 102-112, 2005.

[7] R. Carlson, I. Papamichail, M. Papageorgiou and A. Messmer, "Optimal Motorway Traffic Flow Control Involving Variable Speed Limits and Ramp Metering," *Transportation Science,* vol. 44, no. 2, pp. 238-253, January 2009.

[8] R. Bertini and M. Leal, "Empirical Study of Traffic Features at a Freeway Lane Drop," *Journal of Transportation Engineering,* vol. 131, no. 6, p. 397–407, June 2005.

[9] K. Chung, J. Rudjanakanoknad and M. J. Cassidy, "Relation between traffic density and capacity drop at three freeway bottlenecks," *Transportation Research Part B: Methodological,* vol. 41, no. 1, pp. 82-95, January 2007.

[10] J. Geistefeldt, "Consistency of Stochastic Capacity Estimations," *Transportation Research Record: Journal of the Transportation Research Board,* vol. 2173, no. 1, pp. 89-95, December 2010.

[11] L. Edie, "Discussion of traffic stream measurements and definitions," in *Proceedings of The Second International Symposium on The Theory of Road Traffic Flow*, London, 165.

[12] R. Foote, "Single lane traffic flow control," in *Proceedings of The Second International Symposium on The Theory of Road Traffic Flow*,

London, 1965.

[13] T. Forbes, "Human factor consideration in traffic flow theory," *Highway Research Record,* vol. 15, pp. 60-66, 1963.

[14] H. Yeo, "Asymmetric Microscopic Driving Behavior Theory," University of California, Berkeley, 2008.

[15] M. J. Cassidy and R. L. Bertini, "Some traffic features at freeway bottlenecks," *Transportation Research Part B: Methodological,* vol. 33, no. 1, pp. 25-42, February 1999.

[16] B. Persaud, S. Yagar and R. Brownlee, "Exploration of theBreakdown Phenomenon in Freeway Traffic," *Transportation Research Record: Journal of the Transportation Research Board,* vol. 1634, no. 1, pp. 64-69, Januray 1998.

[17] J. A. Laval and C. F. Daganzo, "Lane-changing in traffic streams," *Transportation Research Part B: Methodological,* vol. 40, no. 3, pp. 251-264, March 2006.

[18] J. A. Laval and L. Leclercq, "Microscopic modeling of the relaxation phenomenon using a macroscopic lane-changing model," *Transportation Research Part B: Methodological,* vol. 42, no. 6, pp. 511-522, July 2008.

[19] M. Papageorgiou, E. Kosmatopoulos and I. PapaMichail, "Effects of variable speed limits on motorway traffic flow," *Transportation Research Record: Journal of the Transportation Research Board,* vol.

2047, pp. 37-48, 2008.

[20] D. Branston, "Models of Single Lane Time Headway Distributions," *Transportation Science,* vol. 10, no. 2, pp. 125-148, May 1976.

[21] W. Brilon, J. Geistefeldt and H. Zurlinden, "Implementing the Concept of Reliability for Highway Capacity Analysis," *Transportation Research Record: Journal of the Transportation Research Board,* vol. 2027, no. 1, pp. 1-8, December 2007.

[22] J. Kim, H. S. Mahmassani and J. Dong, "Likelihood and Duration of Flow Breakdown," *Transportation Research Record: Journal of the Transportation Research Board,* vol. 2188, no. 1, pp. 19-28, December 2010.

[23] E. Kwon, D. Brannan , K. Shouman, C. Isackson and B. Arseneau, "Development and field evaluation of variable advisory speed limit system for work zones," *Transportation Research Record: Journal of the Transportation Research Board,* vol. 2015, no. 1, pp. 12-18, 2007.

[24] A. H. Chow, X. Y. Lu and T. Z. Qiu, "Empirical Analysis of Traffic Breakdown Probability Distribution with Respect to Speed and Occupancy," 2009.

[25] S. Ishak, C. Mamidala and Y. Qi, "Stochastic Characteristics of Freeway Traffic Speed During Breakdown and Recovery Periods," *Transportation Research Record: Journal of the Transportation Research Board,* vol. 2178, no. 1, pp. 79-89, December 2010.

[26] Y. Wang and P. A. Ioannou, "A New Model for Variable Speed Limits," in *The Transportation Research Board (TRB) 90th Annual Meeting*, Wangshington D.C., 2011.

[27] P. Lertworawanich and L. Elefteriadou, "A methodology for estimating capacity at ramp weaves based on gap acceptance and linear optimization," *Transportation Research Part B: Methodological,* vol. 37, no. 5, pp. 459-483, June 2003.

[28] P. Lertworawanich and L. Elefteriadou, "Capacity Estimations for Type B Weaving Areas Based on Gap Acceptance," *Transportation Research Record: Journal of the Transportation Research Board,* vol. 1776, no. 1, pp. 24-34, January 2001.

[29] G. Newell, "A simplified car-following theory: a lower order model," *Transportation Research Part B: Methodological,* vol. 36, no. 3, pp. 195-205, March 2002.

[30] S. Ahn, M. J. Cassidy and J. Laval, "Verification of a simplified car-following theory," *Transportation Research Part B: Methodological,* vol. 38, no. 5, pp. 431-440, June 2004.

[31] T. Kim and H. Zhang, "A stochastic wave propagation model," *Transportation Research Part B: Methodological,* vol. 42, no. 7-8, pp. 619-634, August 2008.

[32] J. A. Laval and L. Leclercq, "A Mechanism to Describe the Formation and Propagation of Stop-and-go Waves in Congested Freeway Traffic,"

Philosophical Transactions of the Royal Society, vol. 368, no. 1928, pp. 4519-4541, October 2010.

[33] G. Newell, "Instability in dense highway traffic, a review," in *Proceedings of The Second International Symposium on The Theory of Road Traffic Flow*, London, 1965.

[34] J. Treiterer and J. Myers, "The hysteresis phenomenon in traffic flow," in *Proceedings of the sixth International Symposium on Transportation and Traffic Theory*, Sydney, 1974.

[35] M. Zhang, "A mathematical theory of traffic hysteresis," *Transportation Research Part B: Methodological, Volume 33,* vol. 33, no. 1, pp. 1-23, February 1999.

[36] H. Zhang and T. Kim, "A car-following theory for multiphase vehicular traffic flow," *Transportation Research Part B: Methodological*, vol. 39, no. 5, pp. 385-399, June 2005.

[37] X. Chen, L. Li and Z. Li, "Phase Diagram Analysis Based on a Temporal-Spatial Queueing Model," *IEEE Transactions Intelligent Transportation Systems,* vol. 13, no. 4, pp. 1705-1716, December 2012.

[38] C. Wang and B. Coifman, "The Effect of Lane-Change Maneuvers on a Simplified Car-Following Theory," *Intelligent Transportation Systems, IEEE Transactions*, vol. 9, no. 3, pp. 523-535, September 2008.

[39] P. Hidas, "Modelling vehicle interactions in microscopic simulation of merging and weaving," *Transportation Research Part C: Emerging*

Technologies, vol. 13, no. 1, pp. 37-62, February 2005.

[40] H. Yeo, A. Skabardonis, J. Halkias, J. Colyar and V. Alexiadis, "Oversaturated Freeway Flow Algorithm for Use in Next Generation Simulation," *Transportation Research Record: Journal of the Transportation Research Board,* vol. 2088, no. 1, pp. 68-79, December 2008.

[41] P. Rämä, " Effects of weather-controlled variable speed limits and warning signs on driver behavior," *Transportation Research Record,* vol. 1689, pp. 53-59, 1999.

[42] J. A. Laval, "Hybrid Models of Traffic Flow:Impacts of Bounded Vehicle Accelerations," 2004.

[43] "Traffic Management Configurator," [Online]. Available: http://www.smartmicro.de/index.php/traffic-radar/traffic-management-configurator. [Accessed 5 August 2013].

[44] A. Duret, C. Buisson and N. Chiabaut, "Estimating Individual Speed-Spacing Relationship and Assessing Ability of Newell's Car-Following Model to Reproduce Trajectories," *Transportation Research Record: Journal of the Transportation Research Board,* vol. 2088, no. 1, pp. 188-197, December 2008.

[45] M. Hadiuzzaman, J. Fang, Y. Luo and T. Z. Qiu, "Relative Contribution of Speed Limit Compliance and Variable Speed Limit Control Strategy on Improving Freeway Mobility and Safety," in

Submitted to Transportation Research Board, Wangshiton D.C., 2014.

[46] R. L. Bertini, "Toward the systematic diagnosis of freeway bottleneck activation," in *Intelligent Transportation Systems, 2003. Proceedings. 2003 IEEE*, Shanghai, 2003.